Characterizing Chromium Isotope Fractionation During Reduction of Cr(VI): Batch and Column Experiments

by

Julia Helen Jamieson-Hanes

A thesis
presented to the University of Waterloo
in fulfillment of the
thesis requirement for the degree of
Master of Science
in
Earth Sciences

Waterloo, Ontario, Canada, 2012

Author's Declaration

I hereby declare that I am the sole author of this thesis. This is a true copy of the thesis, including any required final revisions, as accepted by my examiners.

I understand that my thesis may be made electronically available to the public.

Abstract

Chromium (VI) is a pervasive groundwater contaminant that poses a considerable threat to human health. Remediation techniques have focused on the reduction of the highly mobile Cr(VI) to the sparingly soluble, and less toxic, Cr(III) species. Traditionally, remediation performance has been evaluated through the measurement of Cr(VI) concentrations; however, this method is both costly and time-consuming, and provides little information regarding the mechanism of Cr(VI) removal. More recently, Cr isotope analysis has been proposed as a tool for tracking Cr(VI) migration in groundwater. Redox processes have been shown to produce significant Cr isotope fractionation, where enrichment in the $^{53}Cr/^{52}Cr$ ratio in the remaining Cr(VI) pool is indicative of a mass-transfer process. This thesis describes laboratory batch and column experiments that evaluate the Cr isotope fractionation associated with the reduction of Cr(VI) by various materials and under various conditions.

Laboratory batch experiments were conducted to characterize the isotope fractionation during Cr(VI) reduction by granular zero-valent iron (ZVI) and organic carbon (OC). A decrease in Cr(VI) concentrations was accompanied by an increase in $\delta^{53}Cr$ values for the ZVI experiments. Data were fitted to a Rayleigh-type curve, which produced a fractionation factor $\alpha = 0.9994$, suggesting a sorption-dominated removal mechanism. Scanning electron microscopy (SEM), X-ray absorption near-edge structure (XANES) spectroscopy, and X-ray photoelectron spectroscopy (XPS) indicated the presence of Cr(III) on the solid material, suggesting that reduction of Cr(VI) occurred. A series of batch experiments determined that reaction rate, experimental design, and pre-treatment of the ZVI had little to no effect on the Cr isotope fractionation. The interpretation of isotope results for the organic carbon experiments

was complicated by the presence of both Cr(VI) and Cr(III) co-existing in solution, suggesting that further testing is required.

A laboratory column experiment was conducted to evaluate isotopic fractionation of Cr during Cr(VI) reduction by OC under saturated flow conditions. Although decreasing dissolved Cr(VI) concentrations also were accompanied by an increase in δ^{53}Cr values, the isotope ratio values did not fit a Rayleigh-type fractionation curve. Instead, the data followed a linear regression equation yielding $\alpha = 0.9979$. Solid-phase analysis indicated the presence of Cr(III) on the surface of the OC. Both the results of the solid-phase Cr and isotope analyses suggest a combination of Cr(VI) reduction mechanisms, including reduction in solution, and sorption prior to reduction. The linear characteristic of the δ^{53}Cr data may reflect the contribution of transport on Cr isotope fractionation.

Acknowledgements

I would like to extend my sincerest thanks to my supervisor, Dr. David Blowes, for sparking my interest in non-traditional stable isotopes, and for providing just the right balance of support and independence over the course of my degree. I would also like to thank my committee members, Dr. Carol Ptacek and Dr. Vassili Karanassios, for sharing their valuable input and their passion for research.

Funding for this research was provided by a NSERC Discovery Grant held by David Blowes, with further support awarded through a NSERC Alexander Graham Bell Canada Graduate Scholarship and an Ontario Graduate Scholarship. Thanks also to Dr. Yeongkyoo Kim from Kyungpook National University in Korea for providing his column samples for isotope analysis.

Many thanks to the GRIME research group members, past and present, for creating such a supportive and enthusiastic work environment. In particular, thanks to Jeff Bain and Laura Groza for technical and analytical support, Rich Amos for patiently answering all my questions about MIN3P, Krista Paulson for helping me get through many long hours in the glove box, and Matt Lindsay for making me really think about my research. Special thanks to Blair Gibson for teaching me how to use the Neptune, and for the regular enthusiastic research discussions – you'll turn me into an analytical chemist yet! Thanks also to the other friends I have made along the way, including Krista Desrochers, Stacey Hannam, and Corina McDonald, who were always happy to share the good times and the bad.

None of this would have been possible without the support of my family. I am very grateful to my parents, Heather and John, for instilling in me the passion for discovery and the

work ethic I needed to make it to this point. You were always ready to be exactly who I needed at the time, whether loving parent or curious scientist. Big thanks also to my sister, Jean, for sharing her own experiences with me and helping me to keep it all in perspective.

Finally, my sincerest thanks to my partner, Matt, to whom I owe my sanity. You kept me grounded and supported me at every step, even when I was spending more time in the lab than at home. Thank you for your patience and encouragement, you always knew I would make it.

Dedication

For my boy.

Table of Contents

List of Figures

List of Tables

List of Abbreviations

Alk	alkalinity (in units of mg L^{-1} $CaCO_3$)
BET	Brunauer-Emmett-Teller
BSE	backscatter electron
DI	deionized
DOC	dissolved organic carbon
EDS	energy dispersive spectroscopy
FE-SEM	field emission-scanning electron microscopy
GSE-CARS	GeoSoilEnviro-Center for Advanced Radiation Sources
HEPA	High-Efficiency Particulate Air
ICP-OES	inductively-coupled plasma optical emission spectrometry
ICP-MS	inductively-coupled plasma mass spectrometry
MC-ICP-MS	multi-collector inductively-coupled plasma mass spectrometry
MDL	method detection limit
N/A	parameter not measured
N/D	below method detection limit
NIST	National Institute of Standards and Technology
OC	organic carbon
PE	polyethylene
PET	polyethylene terephthalate
PRB	permeable reactive barrier
PV	pore volume

TIMS	thermal-ionization mass spectrometry
SEM	scanning electron microscopy
SI	saturation index
SPE	solid phase extraction
SRM	standard reference material
SSW	Surface Science Western
XANES	X-ray absorption near edge structure
XPS	X-ray photoelectron spectroscopy
XRF	X-ray fluorescence
ZVI	zero-valent iron

Chapter 1:

Introduction

Chromium (VI) is a highly toxic and mobile groundwater contaminant that has been traditionally remediated by reduction to the sparingly soluble, and less toxic, Cr(III) species. Recent advances in analytical techniques have revealed that reduction of Cr(VI) generates Cr isotope fractionation that can be used to assess the extent of reduction (Ellis et al., 2002). Combining Cr isotope measurements with traditional Cr(VI) concentration measurements and solid-phase analyses may provide a rapid and cost-effective method for tracking the migration of Cr(VI) in groundwater. The primary goal of the research presented in this thesis was to characterize the Cr isotope fractionation during the reduction of Cr(VI) by two common reactive materials, granular zero-valent iron (ZVI) and organic carbon (OC), and to evaluate the potential influence of transport on Cr isotope fractionation under saturated flow conditions. This chapter provides essential background information on the behaviour of Cr(VI) in groundwater, an overview of Cr(VI) treatment by ZVI and OC, and a brief review of the current research on Cr isotope fractionation.

1.1 Background

1.1.1 Cr(VI) in Groundwater

Hexavalent chromium (Cr(VI)) is a common groundwater contaminant of major concern to human health. While trivalent chromium (Cr(III)) is an essential micronutrient, Cr(VI) is both a mutagen and a carcinogen (Losi et al., 1994), with the potential to cause oxidative damage to

DNA in the human body (O'Brien and Kortenkamp, 1994). Although it can be derived from natural geological sources, much of the Cr(VI) released into the environment is a by-product of industrial activities, such as leather tanning and electroplating (Blowes, 2002). In an extreme example, from a site in Oregon, USA, there were Cr(VI) concentrations of up to 14,600 mg L^{-1} in the groundwater as a result of a leaky process tank at a plating facility (Palmer and Wittbrodt, 1991). In its oxidized form, Cr(VI) exists in groundwater as $HCrO_4^-$, CrO_4^{2-}, and $Cr_2O_7^{2-}$ oxyanions, and is highly mobile and toxic (Losi et al., 1994). Treatment of Cr(VI) in groundwater is generally accomplished through reduction, as Cr(III) is both less mobile and less toxic (Losi et al., 1994).

Multiple remediation techniques exist to effect the reduction to Cr(III). These include pump and treat, permeable reactive barriers (PRBs), direct injection of a reductant, and natural attenuation by the substrate. Natural attenuation is preferable because it is low-cost and non-invasive (Blowes, 2002). A wide variety of materials can be used as electron donors for the reduction of Cr(VI), including aqueous Fe(II) (Eary and Rai, 1988; Sevim and Demir, 2008), granular zero-valent iron (Blowes et al., 1997; Dutta et al., 2010), organic carbon (Bolan et al., 2003; Park et al., 2008), and certain bacteria (Lovley and Phillips, 1994; Cummings et al., 2006). In all cases the goal is reduce Cr(VI) to the less toxic Cr(III) form through the following reaction (Losi et al., 1994):

(1.1) $$HCrO_4^- + 7H^+ + 3e^- \rightarrow Cr^{3+} + 4H_2O$$

Aqueous Cr(III) generated during Cr(VI) reduction is readily precipitated as $Cr(OH)_3$ under moderate to high pH conditions (Rai et al., 1987; Palmer and Wittbrodt, 1991):

(1.2) $$Cr^{3+} + 3OH^- \rightarrow CrOH_3(s)$$

Once immobilized through precipitation, the reduced Cr(III) remains in situ, and the site is considered to be adequately remediated. In some treatment systems, further steps may be taken to remove the precipitated Cr(III) through filtration or sedimentation (Losi et al., 1994).

1.1.2 Treatment of Cr(VI) by Zero-Valent Iron and Organic Carbon

Granular zero-valent iron (ZVI) is frequently used for the treatment of Cr(VI) in groundwater, particularly in the construction of permeable reactive barriers (PRBs) (Blowes et al., 1997; Blowes et al., 2000; Jeen et al., 2008). The ZVI is available through commercial sources as scrap granular Fe from industrial activities, but can also be generated in the laboratory, generally as micro- or nano-sized particles (Gheju, 2011). Reduction of Cr(VI) is achieved through the corrosion of Fe, which occurs readily under anaerobic conditions and releases dissolved Fe(II) (Blowes et al., 2000):

(1.3) $$Fe^0(s) + 2H^+ \rightarrow Fe^{2+} + H_2(aq)$$

The aqueous Fe(II) is then available as an electron donor for the reduction of Cr(VI) to Cr(III), which is coupled with the oxidation of Fe (Blowes et al., 1997):

(1.4) $$Cr(VI)(aq) + Fe(II)(aq) \rightarrow Cr(III)(aq) + Fe(III)(aq)$$

In addition to the precipitation of $Cr(OH)_3$, reduced Cr(III) also has been observed to co-precipitate with Fe(III) in the form of hydroxides or (oxy)hydroxides (Blowes et al., 1997):

(1.5) $$(1-x)Fe^{3+} + xCr^{3+} + 3H_2O \rightarrow (Fe_{(1-x)}Cr_x)(OH)_3(s) + 3H^+$$

(1.6) $$(1-x)Fe^{3+} + xCr^{3+} + 2H_2O \rightarrow Fe_{(1-x)}Cr_xOOH(s) + 3H^+$$

Organic carbon also is a common material used for the treatment of Cr(VI) in groundwater, and can be derived from a wide range of sources including manure, sawdust, pine needles, and fungal biomass (Bolan et al., 2003; Park et al., 2005; Park et al., 2008). The reduction of Cr(VI) is coupled with organic carbon degradation, which can be described by the following reaction (Bolan et al., 2003):

(1.7) $$3CH_2O + 2Cr_2O_7{}^{2-} + 16H^+ \rightarrow 4Cr^{3+} + 3CO_2 + 11H_2O$$

The application of organic carbon for Cr(VI) remediation is potentially advantageous, as the biomaterials are inexpensive and the reaction does not produce the large volumes of secondary waste generated through other techniques (Park et al., 2005).

1.1.3 Chromium Isotopes

Chromium has four stable isotopes, ^{50}Cr, ^{52}Cr, ^{53}Cr, and ^{54}Cr, with natural abundances of 4.35%, 83.8%, 9.5%, and 2.37%. Following the complete radioactive decay of ^{53}Mn (half-life of 3.7 Myr) to ^{53}Cr in the early history of the Earth, materials of terrestrial origin should be expected to exhibit identical Cr isotope signatures (Frei and Rosing, 2005). However, certain processes have been observed to fractionate Cr isotopes. In particular, the transition from tetrahedrally-coordinated Cr(VI) to octrahedrally-coordinated Cr(III) during Cr reduction is predicted to cause the largest change in isotope composition (Schauble et al., 2004). The lighter isotope, ^{52}Cr, is preferentially reduced due to its higher vibrational energy (Schauble et al., 2004), resulting in an enrichment of ^{53}Cr in the remaining unreacted Cr(VI) pool. This enrichment is measured as the change in the ratio of ^{53}Cr/^{52}Cr, and is expressed as δ^{53}Cr in units of per mil (‰) relative to a standard according to the following equation:

(1.8)
$$\delta^{53}Cr = \left[\frac{\left(^{53}Cr/^{52}Cr\right)_{sample} - \left(^{53}Cr/^{52}Cr\right)_{standard}}{\left(^{53}Cr/^{52}Cr\right)_{standard}}\right] \times 1000$$

where positive δ^{53}Cr values in the remaining Cr(VI) are indicative of reduction.

Analytical advances have been made in the field of non-traditional stable isotope geochemistry such that changes in the δ^{53}Cr signature can be measured (Ellis et al., 2002). Simultaneous measurement of all four stable Cr isotopes is crucial for detecting the relatively small changes in the ^{53}Cr/^{52}Cr ratio during Cr isotope fractionation. Two types of instruments

are currently used for such analysis of Cr isotopes: thermal-ionization mass spectrometers (TIMS) and multi-collector inductively-coupled plasma mass spectrometers (MC-ICP-MS).

1.1.4 Tracking Cr(VI) Migration in Groundwater

Traditionally, Cr(VI) concentration measurements have been used to monitor the extent of Cr(VI) remediation (Blowes, 2002). More recently, the application of Cr isotopes has been proposed as a beneficial tool for tracking Cr(VI) migration in groundwater (Blowes, 2002; Ellis et al., 2002). Whereas concentration measurements describe only the changes in Cr(VI), Cr isotope fractionation can provide more complete information on the conditions in the subsurface and the presence of any mass-transfer processes (Blowes, 2002). Laboratory experiments have demonstrated that the degree of δ^{53}Cr enrichment is dependent on the reductant and the mechanism of Cr(VI) removal (Ellis et al., 2002, 2004; Sikora et al., 2008; Berna et al., 2010; Zink et al., 2010; Døssing et al., 2011), suggesting that careful evaluation of potential remediation materials will be necessary prior to the application of this new tool in the field.

The first published Cr isotope results appear in Ellis et al. (2002), where a significant enrichment in δ^{53}Cr was observed during Cr(VI) reduction in laboratory batch experiments using magnetite and sediment slurries. The isotope data follow a Rayleigh-type fractionation curve, which assumes that the product (Cr(III)) is completely isolated from the reactant (Cr(VI)), and results in an exponential increase in δ^{53}Cr as the fraction of remaining Cr(VI) decreases. A kinetic fractionation factor (α) can be calculated to describe the extent of fractionation using the following equation (Clark and Fritz, 1997):

(1.9) $$\frac{R}{R_0} = f^{(\alpha-1)}$$

where R is the isotope ratio, R_0 is the initial isotope ratio, and f is the fraction of Cr(VI) remaining in solution. The work by Ellis et al. (2002) establishes α = 0.9965 for Cr(VI) removal by magnetite, which is attributed to reduction in solution. Similar batch experiments using a variety of materials as the electron donor have generated α values ranging from 0.9950 to 0.9985 (Table 1.1). Subsequent work by Ellis et al. (2004) investigated the effect of sorption on Cr isotope fractionation. As predicted by Schauble et al. (2004), a lack of change in coordination number results in little to no fractionation (Table 1.1). Using α = 0.9965 for reduction in solution, and α = 1.0000 for sorption, Døssing et al. (2011) attributed their α value of 0.9985 to a mixture of mechanisms: direct Cr(VI) reduction by $Fe(II)_{aq,}$ and sorption of Cr(VI) to green rust followed by reduction that did not fractionate the remaining Cr(VI) pool.

Observations of enriched $\delta^{53}Cr$ values in field samples have been reported in the literature (Ellis et al., 2002; Izbicki et al., 2008; Berna et al., 2010; Raddatz et al., 2011). The samples were obtained from various sources, including groundwater contaminated by plating waste in California (Ellis et al., 2002; Berna et al., 2010), laboratory waste in Idaho (Raddatz et al., 2011), and natural geological sites in the Mojave Desert (Izbicki et al., 2008). Attempts were made to use the Cr isotope data to determine the extent of Cr(VI) reduction, but interpretation was found to be convoluted due to system heterogeneities and high background Cr(VI) concentrations (Izbicki et al., 2008; Berna et al., 2010). In addition, the influence of

transport on isotope fractionation during Cr(VI) reduction under saturated flow conditions is largely unknown.

1.2 Research Objectives

The primary objectives of the research described in this thesis are to enhance the understanding of Cr isotope fractionation during treatment by various reactive materials to more effectively use Cr isotopes as a tool for tracking Cr(VI) migration in groundwater. Used in tandem with traditional geochemical measurements and solid-phase analyses, Cr isotopes can provide more detailed information about the geochemical processes occurring during Cr(VI) treatment. The ultimate goal of this type of research into Cr isotopes is to develop a more rapid and cost-effective technique for evaluating the performance of Cr(VI) treatment projects in the field. Specific objectives of the research for this thesis included:

- Characterization of the Cr isotope fractionation during Cr(VI) treatment by granular ZVI and organic carbon, and assessment of the effect of varying experimental conditions on fractionation.
- Evaluation of the Cr isotope fractionation during Cr(VI) treatment by organic carbon under saturated flow conditions that more closely replicate field conditions.

1.3 Thesis Organization

This thesis is presented as two research papers related to the objectives outlined in the previous section. The first paper, presented as Chapter 2, describes laboratory batch experiments conducted to evaluate the Cr isotope fractionation during Cr(VI) treatment by granular zero-valent iron and organic carbon under a variety of conditions. Chapter 3 presents data from a column study designed to investigate Cr isotope fractionation during Cr(VI) treatment by organic carbon under saturated flow conditions. The final chapter, Chapter 4, presents a summary of findings from the two research papers and recommendations for future research.

Table 1.1 Summary of fractionation factors (α) from the Cr isotope literature.

Material	α	**Mechanism**	**Source**
magnetite; pond sediment; estuarine sediment	0.9965; 0.9965; 0.9967	reduction in solution	Ellis et al. (2002)
goethite; alumina	1.0000	sorption	Ellis et al. (2004)
Shewanella oneidensis	0.9959; 0.9983	biotic reduction	Sikora et al. (2008)
sediment slurry	0.9969; 0.9976	reduction by green rust	Berna et al. (2010)
H_2O_2	0.9965; 0.9950	reduction in solution	Zink et al. (2010)
$Fe(II)_{(aq)}$	0.9964; 0.9985	reduction in solution; mix of reduction in solution and sorption followed by reduction	Døssing et al. (2011)

Chapter 2:

Isotopic Fractionation During Reduction of Cr(VI) by Zero-Valent Iron and Organic Carbon: Batch Experiments

2.1 Summary

The application of chromium isotopes for tracking Cr(VI) migration in groundwater requires careful characterization of the isotope fractionation curve. A series of laboratory batch experiments was conducted to evaluate the Cr isotope fractionation associated with Cr(VI) reduction by granular zero-valent iron and organic carbon. A 50 mg L^{-1} Cr(VI) solution was introduced to each reactive material in a series of six batch experiments that compared variable experimental conditions, including pre-treatment of the solids, experimental design, reaction rates, and solution matrix. Isotope measurements were performed on the aqueous samples, along with analyses of pH, Eh, alkalinity, and dissolved cations and anions. The batch systems containing zero-valent iron exhibited a decrease in dissolved Cr(VI) concentrations with an increase in $\delta^{53}Cr$ that followed a Rayleigh-type trend with an average fractionation factor (α) of 0.9994, suggesting a sorption-dominated removal mechanism. Analysis of the solid material by scanning electron microscopy (SEM) with energy dispersive spectroscopy (EDS) indicated that solid-phase Cr was widely distributed across the surface of the reactive material. Chromium(VI) reduction was suggested for all experiments by the presence of Cr(III) on the surface of the solids, measured by X-ray absorption near edge structure (XANES) spectroscopy and X-ray photoelectron spectroscopy (XPS). Interpretation of isotope results for the organic carbon experiments was convoluted by the presence of both Cr(VI) and Cr(III) in solution, indicating that changes to the sample preparation method are required to analyze the isotope composition of the Cr(VI) in these samples. Results from this study demonstrate that batch experiments are essential to evaluate Cr isotope fractionation for each reactive material prior to

applying Cr isotopes as a tool for tracking Cr(VI) migration in groundwater. In addition, this study shows that combining different analytical techniques, such as aqueous, solid-phase, and isotope measurements, may provide data that either reinforces an initial hypothesis or generates complementary information.

2.2 Introduction

Chromium (VI) is a highly soluble and mobile groundwater contaminant most commonly derived from tanning and electroplating (Blowes, 2002). This oxidized form of Cr is toxic, existing in groundwater as $HCrO_4^-$, CrO_4^{2-}, and $Cr_2O_7^{2-}$ oxyanions (Losi et al., 1994). Treatment methods focus on the reduction of Cr(VI) to the less soluble Cr(III), which is readily precipitated and immobilized under mildly acidic, neutral, and alkaline conditions (Rai et al., 1987; Palmer and Wittbrodt, 1991). Electron donors for Cr(VI) reduction include aqueous Fe(II) (Eary and Rai, 1988; Sevim and Demir, 2008), granular zero-valent iron (Blowes et al., 1997; Dutta et al., 2010), organic carbon (Bolan et al., 2003; Park et al., 2008), and certain bacteria (Lovley and Phillips, 1994; Cummings et al., 2006).

Chromium has four stable isotopes, ^{50}Cr, ^{52}Cr, ^{53}Cr, and ^{54}Cr, with natural abundances of 4.35%, 83.8%, 9.5%, and 2.37%. Redox changes, such as the transition from tetrahedrally-coordinated Cr(VI) to octrahedrally-coordinated Cr(II), can cause a shift in the $^{53}Cr/^{52}Cr$ ratio (Schauble et al., 2004). The lighter isotopes are preferentially reduced, resulting in an enrichment of ^{53}Cr relative to ^{52}Cr in the unreacted Cr(VI) and a corresponding depletion in the reduced Cr(III). Isotopic enrichment of Cr(VI) is indicative of mass-transfer processes such as reduction, therefore the measurement of stable Cr isotopes has been proposed as a tool for

tracking Cr(VI) migration in groundwater (Blowes, 2002; Ellis et al., 2002). Observations of enriched δ^{53}Cr values have been reported from various field settings (Ellis et al., 2002; Izbicki et al., 2008; Berna et al., 2010; Raddatz et al., 2011), but interpretation of these results remains challenging due to heterogeneity of the substrate and high natural background Cr(VI) concentrations (Izbicki et al., 2008; Berna et al., 2010).

Recent laboratory studies have demonstrated that the extent of isotopic fractionation relies on the type of electron donor involved with Cr(VI) reduction (Ellis et al., 2002, 2004; Sikora et al., 2008; Berna et al., 2010; Zink et al., 2010; Døssing et al., 2011). A measurable enrichment of δ^{53}Cr was first reported by Ellis et al. (2002) as a result of Cr(VI) reduction by magnetite. Similar results were later observed in sediment slurry batch experiments from Berna et al. (2010) and reduction by aqueous Fe(II) conducted by Døssing et al. (2011). In contrast, Ellis et al. (2004) demonstrated that little to no isotope fractionation occurs during sorption of Cr(VI) by minerals such as goethite and alumina, likely because no change in coordination occurs. In this study, batch experiments were conducted to assess the degree of Cr isotope fractionation during Cr(VI) treatment by granular zero-valent iron and organic carbon. Additional potential influences were also considered, including pre-treatment of the zero-valent iron, experimental design, and changes in reaction rate. Analyses of water chemistry, solid-phase mineralogy, and stable Cr isotopes were performed to evaluate the results.

2.3 Laboratory Methods

2.3.1 Experimental Setup

Laboratory batch experiments were conducted using both granular zero-valent iron (ZVI; Connelly GMP, Chicago, IL, USA) and organic carbon (OC) as mixed deciduous-tree leaf mulch from a local landfill (Region of Waterloo Waste Management, Waterloo, ON, Canada) to evaluate the Cr isotope fractionation during Cr(VI) reduction. All of the experiments were carried out in an anaerobic chamber (Coy Laboratory Products Inc., Grass Lake, MI, USA) under a 3.5% H_2/balance N_2 atmosphere. Varying experimental conditions were tested, including single batch flask vs. multiple flask treatment, untreated vs. pre-treated ZVI, and changes in the mass of treatment media relative to the initial volume of solution (Table 2.1). Replicate experiments (designated 'A' and 'B') were performed to assess reproducibility for all experiment types except for a multi-flask experiment using zero-valent iron in artificial groundwater (ZVI-MP). Single-flask experiments, where multiple samples were collected from a single batch reaction flask over time, were performed using one 400 mL amber glass bottle (VWR International, Radnor, PA, USA). For the multi-flask experiments, between five and twenty 250 mL amber glass bottles were used for each experiment and one bottle was randomly selected and sampled sacrificially at each time step. At several time steps in each multi-flask experiment, duplicate bottles were sampled simultaneously to assess reproducibility within the experiment.

Connelly ZVI was used as-received for batch experiments ZVI-S10, ZVI-S100, and ZVI-M. A separate experiment (ZVI-MP) was performed to test the treatment capability of

ZVI after removal of the oxide coatings. The removal of the oxide coatings was intended to simulate the removal of oxidation products during aging of a permeable reactive barrier. The ZVI was sieved at 16 – 60 mesh (0.25 – 1.19 mm) and then soaked in 1 M HCl. The acid was periodically decanted and replaced over the course of 6-7 hours, resulting in the ZVI changing in color from brown to black. After a final 1 M HCl rinse, the ZVI was submerged in 0.1 M HCl and transported into the anaerobic chamber, where it was rinsed with Ar-purged high-purity Milli-Q® water and vacuum-filtered. The cleaned ZVI was packed into a 20 x 5 cm Plexiglas® column through which Ar-purged deionized (DI) water was pumped for 2 weeks, followed by Ar-purged $CaCO_3$-saturated DI water for 4 weeks. Following the development of reducing conditions as indicated by redox measurements of the effluent, the column was disassembled in the anaerobic chamber and the pre-treated ZVI was weighed out into amber glass bottles. Moisture content of the pre-treated ZVI was determined both by oven-drying and freeze-drying.

The organic carbon was sieved at < 10 mesh (2.00 mm) to remove large particles such as twigs, and then covered to prevent drying. Moisture content of the OC was determined by weighing a representative sample before and after heating for 24 hours in a 100°C oven. Appropriate masses of each reactive material were weighed out into amber glass bottles, which were then placed in the anaerobic chamber and allowed to equilibrate.

A 50 mg L^{-1} Cr(VI) input solution was prepared by dissolving $K_2Cr_2O_7$ in either DI water or $CaCO_3$-saturated DI water (Table 2.1). The input solution was purged with anaerobic grade $Ar_{(g)}$ in the anaerobic chamber for 2-3 hours prior to use. Batch experiments were initialized by adding an appropriate volume of input solution to each of the reaction bottles. A

control bottle was included in each experiment in which Cr-free water was added to the solids to monitor for Cr contamination in the reactive material. Initially the reaction flasks were agitated on an orbital shaking table in the anaerobic chamber (replicate 'A'). Subsequent bottles were hand tumbled twice a day at regular intervals (replicate 'B'). The ZVI-MP batch experiment was also hand tumbled.

2.3.2 Water Sampling and Analysis

Aqueous sampling was performed in the anaerobic chamber using disposable polyethylene (PE) syringes (BD, Franklin Lakes, NJ, USA). Samples were drawn directly out of the single-flask experiment bottles, while the multi-flask bottles were vacuum-filtered through 0.45 μm cellulose acetate filters (Whatman, UK) to halt the reaction prior to sampling. Samples from the OC-M experiments were strongly coloured orange-brown even after filtration, suggesting the presence of dissolved organic carbon (DOC). Measurements of pH and redox potential (Eh) were immediately performed in the anaerobic chamber on unfiltered samples. The pH was determined using an Orion Ross 815600 electrode (Thermo Scientific, Waltham, MA, USA), which was calibrated with standard pH 4 and 7 buffers. The performance of the Eh electrode (Orion 9678, Thermo Scientific) was checked with Zobell's solution (Nordstrom, 1977) and Light's solution (Light, 1972) prior to sampling. Alkalinity measurements were performed on sample aliquots filtered through 0.2 μm Supor membrane filters (Acrodisc, Pall, UK) by adding the bromocresol green-methyl red indicator and titrating to the end point with H_2SO_4. Due to volume limitations, pH, Eh, and alkalinity measurements were not performed on single-flask experiments. Filtered sub-samples (0.2 μm) were retained unacidified in refrigerated PE

bottles (Thermo Scientific Nalgene, Rochester, NY, USA) for anion analyses, while samples for cation and Cr isotope analyses were acidified to pH < 2 with HNO_3 prior to refrigeration. Unacidified samples were promptly analyzed for Cr(VI) concentrations on a Hach DR/2010 spectrophotometer at 540 nm using the 1,5-diphenylcarbohydrazide method (Greenberg et al., 1992). Concentrations of inorganic anions were determined by ion chromatography (Dionex DX 600). Cation concentrations were measured by inductively coupled plasma-optimal emission spectrometry (Thermo Scientific iCAP 6500) and inductively coupled plasma-mass spectrometry (Thermo Scientific XSeries 2) on samples acidified to pH < 2 with trace-metal grade HNO_3.

2.3.3 Chromium Isotope Analysis

Acidified samples were purified and pre-concentrated for Cr isotope analysis using an ion-exchange separation method modified from Ball and Bassett (2000). All sample preparations were carried out in a HEPA-filtered laminar flow hood. Sample aliquots containing 20 μg Cr were mixed with 8 μg Cr from a ^{50}Cr-^{54}Cr double spike solution composed of enriched Cr metal (ISOFLEX USA, San Francisco, CA, USA) dissolved in 2 N HNO_3. High purity Milli-Q® water was added to the sample-spike mixture to obtain a total volume of 9 mL. Ammonium persulfate (Sigma-Aldrich, St. Louis, MO, USA) was added to each sample (1 mL of 0.2 mol L^{-1}), and the mixture was gently boiled for ~25 minutes to oxidize the Cr (Schoenberg et al., 2008). Incomplete oxidation was observed for the OC samples, presumably due to interferences from DOC. Modifications were made such that 1 mL of saturated ammonium

persulfate was added to the sample-spike mixture for the high DOC samples, and the samples were processed until the recovery was sufficient for isotope analysis.

A 3 mL SPE column (Supelco, Bellefonte, PA, USA) was loaded with 0.5 mL Bio-Rad AG1-X8 anion exchange resin sandwiched between two 20 μm frits (Supelco, Bellefonte, PA, USA). Preliminary testing revealed that the resin contained trace amounts of Fe and other metals. Prior to addition of the sample, the resin was cleaned by saturating with 2 N HNO_3 for 2 hours and then flushing with additional 2 N HNO_3 and high-purity water to remove these contaminants. The resin was then conditioned by sequentially passing 2 mL each of 6 N, 4 N, 2 N, and 1 N HNO_3, followed by 20 mL of high-purity Milli-Q® water through the column. Oxidized sample-spike mixtures were pipetted onto the exchange resin and flushed with 15 mL of water to remove impurities. The Cr(VI) retained on the exchange resin was reduced to Cr(III) by saturating the resin in 2 N HNO_3 for 2 hours. After reduction the Cr was eluted into a sample vial with 2 N HNO_3 and Milli-Q® to achieve a final concentration of 2 mg L^{-1} Cr and 1 N HNO_3. Purified samples were diluted 1:1 with Milli-Q® prior to analysis. Standards were prepared simultaneously with the unknown samples, following the identical procedure. Two aliquots of the $Cr(NO_3)_3 \cdot 9H_2O$ NIST SRM 979 standard (known isotopic composition) were included in the preparation procedure for every 8 unknown samples. One high-purity Milli-Q® water blank and one sample duplicate were also included at the sample preparation stage.

High-precision Cr isotope measurements were performed by multi-collector inductively-coupled plasma mass spectrometry (Thermo Scientific Neptune) in medium-resolution mode using the stable inlet system (double cyclonic spray chamber). All four stable Cr isotopes (^{50}Cr, ^{52}Cr, ^{53}Cr, and ^{54}Cr) were measured simultaneously along with ^{49}Ti, ^{51}V, and

^{56}Fe to facilitate corrections due to isobaric interferences on ^{50}Cr and ^{54}Cr. Off-centre peak measurements were performed to minimize polyatomic interferences from ^{40}Ar^{14}N on ^{54}Cr and ^{40}Ar^{16}O on ^{56}Fe. Sensitivity on the ^{52}Cr signal was in the range of 4-6 V ppm^{-1}. Integration time was 4.194 seconds, with 1 block of 300 cycles.

The ^{50}Cr-^{54}Cr double spike solution was used to quantify isotope fractionation induced by sample preparation and instrumental mass bias. A double-nested iterative routine modified from Siebert et al. (2001) was implemented to subtract the contribution from Ti, V, and Fe, and extract the composition of the naturally fractionated sample. A 2σ outlier test was performed on the raw data, after which the iterative routine was applied to each of the individual measurements, averaging only the final values. The results are expressed as δ^{53}Cr in per mil (‰) relative to the NIST SRM 979 Cr isotope standard, where:

(2.1)
$$\delta^{53}Cr = \left[\frac{\left(^{53}Cr/^{52}Cr\right)_{sample} - \left(^{53}Cr/^{52}Cr\right)_{standard}}{\left(^{53}Cr/^{52}Cr\right)_{standard}}\right] \times 1000$$

Data were fitted to a Rayleigh distillation model, allowing a kinetic fractionation factor to be calculated as follows (Clark and Fritz, 1997):

(2.2)
$$\frac{R}{R_0} = f^{(\alpha-1)}$$

where R is the isotope ratio, R_0 is the initial isotope ratio, f is the fraction of Cr(VI) remaining in solution, and α is the kinetic fractionation factor. External reproducibility for this method

was calculated to be ±0.05‰ (2σ) on the $^{53}Cr/^{52}Cr$ ratio, determined from daily measurements of SRM 979 prepared with each sample set. Submission of four unknown samples to an independent laboratory for Cr isotope analysis validated the performance of the above method within ±0.06‰ (2σ).

2.3.4 Solid-Phase Sampling and Analysis

The treatment material solids were separated from solution in the anaerobic chamber by vacuum-filtering through a 0.45 μm cellulose acetate filter. Each sample was immediately stored in an 8 mL PE bottle, which was transferred out of the anaerobic chamber in a small sealed container and stored in a freezer within 5-10 minutes of sampling. After freezing overnight, the solids were reintroduced to the anaerobic chamber and the bottles were opened and loaded into glass vessels in preparation for freeze-drying. The samples were then removed from the anaerobic chamber and promptly attached to a freeze-drier (Labconco FreeZone, Kansas City, MO, USA). After drying, the samples were placed back in the anaerobic chamber where the sample bottles were sealed and stored in a vacuum desiccator.

Field emission-scanning electron microscopy (FE-SEM; Leo1530, Carl Zeiss SMT GmbH, Germany) with energy dispersive spectroscopy (EDS; EDAX Pegasus 1200, AMETEK Inc., USA) were used to examine secondary precipitates. The freeze-dried samples were mounted on Al stubs with C tape and coated with a 10-12 nm thick Au layer to ensure conductance. An accelerating potential of 15 kV was used for backscatter electron (BSE) imaging and collection of semi-quantitative EDS spectra.

Synchrotron-based X-ray fluorescence (XRF) and X-ray absorption near edge structure (XANES) spectroscopy were performed at the GSE-CARS beamline 13-BM-D at the Advanced Photon Source, Argonne National Laboratory (Chicago, IL, USA). Several samples were chosen from each experiment, representing both early and late time in the reaction. All sample preparation was performed in the anaerobic chamber. The samples were mounted separately in 1 mm-thick Al sample holders between two layers of Kapton® tape. Reference materials were ground using an acid-washed agate mortar and pestle and passed through a 63 μm stainless steel sieve. These materials were spread onto polyethylene terephthalate (PET) tape (Scotch Magic Tape, 3M, St. Paul, MN, USA), which was layered to a thickness of 300 - 500 μm and sealed between two additional layers of PET tape. Bulk Cr K-edge XANES spectra were collected with an unfocused incident beam (~0.5 × 3 mm). Spectra for samples were collected using a four-element Si detector (Vortex ME-4, SII NanoTechnology USA Inc., Northridge, CA, USA), whereas spectra for reference materials were collected in transmission mode. Replicate scans were averaged and smoothed, and linear combination fitting was performed using the program ATHENA, which is a component of the IFEFFIT software package (Ravel and Newville, 2005).

X-ray photoelectron spectroscopy (XPS) was performed at Surface Science Western (SSW; University of Western Ontario, London, ON, Canada) using a Kratos Axis Ultra X-ray photoelectron spectrometer. Subsamples were transferred into 8 mL PE bottles in the anaerobic chamber and transported to the XPS facility in a sealed container. Samples were exposed to atmospheric oxygen only when they were mounted on PET tape attached to the sample holder immediately prior to analysis. Survey scans and Cr 2p spectra were collected for all samples. In

addition, Fe 2p spectra were collected for the ZVI samples. Processing of the XPS data was performed at SSW.

2.3.5 Geochemical Modeling

Aqueous geochemistry results were modeled using the multi-component reactive transport model MIN3P (Mayer, 1999). Reactions for the corrosion of ZVI coupled with the reduction of Cr(VI) and H_2O implemented in the model were established by Mayer et al. (2001) and subsequently used by Jeen (2005). The reaction describing the degradation of OC coupled with the reduction of Cr(VI) was adapted from Amos et al. (2004). Modeling was used to calculate saturation indices (SI) to identify mineral phases controlling the reactions, including the precipitation of secondary minerals based on the databases from Mayer et al. (2001) and Jeen (2005) and phases observed during analysis of the solid material. Cr(VI) removal rates were calculated from the analyzed aqueous concentrations and adjusted within the model to match the experimental results.

2.4 Results and Discussion

2.4.1 Aqueous Geochemistry

The replicate measurements of aqueous geochemistry and Cr isotope fractionation were in very close agreement for most of the batch experiments. One replicate experiment was chosen for discussion in this study, although the complete results for all experiments can be found in Appendix A. Replicate ‘A’ was selected for the single-flask experiments (ZVI-S10 and ZVI-S100), which were shaken on an orbital shaking table, while replicate ‘B’ was chosen for the

multi-flask experiments (ZVI-M and OC-M), which were hand-tumbled (see Section 2.3.1). Data presented in the figures include results from only the selected replicate experiments. Results differed significantly between the replicate OC-M experiments (OC-MA and OCM-B; Table 2.2); this difference was likely due to the change in shaking technique between the replicate experiments, which resulted in exposure of a greater proportion of the reactive material surface area to the Cr(VI) solution in the second experiment. The lack of reproducibility of the OC-M experiments will be further discussed in Section 2.4.3.4.

Rapid increases in pH were observed for both ZVI and OC experiments (Figure 2.1). Both ZVI-M and OC-M input solutions exhibited slightly acidic pH values (5.44 and 5.39), while the $CaCO_3$-saturated input solution of ZVI-MP was initially slightly alkaline at 8.77. In the absence of $CaCO_3$ (ZVI-M), the pH reached a maximum value of 10.70. This large increase in pH is partly due to the reduction of H_2O, which is characteristic of ZVI corrosion under anaerobic conditions (Blowes et al., 2000):

(2.3) $$Fe^0(s) + 2H^+ \rightarrow Fe^{2+} + H_2(aq)$$

Reduction of Cr(VI) by ZVI also is accompanied by an increase in pH, though the subsequent precipitation of Cr(III)-Fe(III) (oxy)hydroxides produces H^+. Overall, an increase in pH is observed (Blowes et al., 1997; Blowes et al., 2000):

(2.4) $$CrO_4^{2-} + Fe^0 + 8H^+ \rightarrow Fe^{3+} + Cr^{3+} + 4H_2O$$

(2.5) $$(1-x)Fe^{3+} + xCr^{3+} + 2H_2O \rightarrow Fe_{(1-x)}Cr_xOOH(s) + 3H^+$$

An increase in pH also was observed for ZVI-MP. However, in the presence of $CaCO_3$ in solution a lower maximum value of 9.96 was observed at the end of the experiment. An increase in pH results in a shift in the carbonate-bicarbonate (CO_3^{2-}-HCO_3^-) equilibria. Saturation index values indicate that the equilibrating solution was supersaturated with respect to the carbonate minerals calcite ($CaCO_3$) and ferrous hydroxycarbonate ($Fe_2(OH)_2CO_3$). The precipitation and dissolution of these minerals has the potential to buffer the overall pH value in the system (Jeen et al., 2008). The increase in pH up to 9.29 observed in OC-M is characteristic of the degradation of organic carbon coupled with Cr(VI) reduction (Bolan et al., 2003):

(2.6) $$3CH_2O + 2Cr_2O_7^{2-} + 16H^+ \rightarrow 4Cr^{3+} + 3CO_2 + 11H_2O$$

Trends in Eh were less well defined, likely due to the low concentrations of electroactive redox species in solution and the presence of high concentrations of chromate, which causes interferences with the platinum electrode (Nordstrom and Wilde, 2006). Both ZVI-M and OC-M exhibited initial Eh values of 600 mV, which decreased fairly consistently throughout the experiments to 185 mV and 260 mV. The initial Eh of ZVI-MP was slightly lower at 370 mV, dropping as low as -170 mV before ending at 110 mV. In all cases, the redox measurements suggest a relatively weak trend toward reducing conditions.

Total alkalinity increased in both the ZVI-M and OC-M batch systems, from an initial value of 1.5 mg L^{-1} (as $CaCO_3$) to values of 35-40 mg L^{-1} and 135 mg L^{-1}, respectively. High alkalinity values in the OC-M batch experiment can be attributed to organic carbon degradation (Eq. 2.6). In contrast, an initial relatively high total alkalinity of 128 mg L^{-1} for the ZVI-MP experiment was followed by a steady decrease to a final value of 58 mg L^{-1}. This overall decreasing trend is most likely due to carbonate mineral precipitation as a result of increasing pH (Gui et al., 2009). Geochemical modeling indicated a maximum saturation index (SI) of 1.48 for $CaCO_3$ and 0.49 for $Fe_2(OH)_2CO_3$ after 0.2 days. Carbonate precipitation in ZVI-MP is further indicated by the change in aqueous Ca concentration, which was initially 52.7 mg L^{-1} and decreased steadily to below the method quantification limit (MQL) of 0.4 mg L^{-1} by the end of the experiment.

Dissolved metal concentrations varied between the experiment types and throughout each experiment. Concentrations of dissolved metals were very low in the Cr(VI)-DI water input solution. Therefore, any increase in the concentrations of trace metals was assumed to be derived from the reactive material. Aqueous Fe concentrations were low in both ZVI multi-flask experiments, increasing to 30 μg L^{-1} in ZVI-M while remaining below the method detection limit (MDL) of 0.17 μg L^{-1} in ZVI-MP. The control sample for ZVI-M contained 674 μg L^{-1} $Fe_{(aq)}$, suggesting that the low concentrations in the Cr-containing samples were the result of precipitation of Fe, likely as Fe (oxy)hydroxides and Fe hydroxycarbonate in the presence of $CaCO_3$ (Blowes et al., 1997; Jeen et al., 2007). The concentrations of Mg, Mn, and Zn initially increased to maximums of 0.50 mg L^{-1}, 0.42 mg L^{-1}, 0.07 mg L^{-1}, respectively, in the ZVI-S100 experiment, followed by a fairly steady decrease as the reaction progressed.

Similar trends were observed in the other ZVI experiments, although the experiments with a smaller mass of reactive material resulted in lower aqueous concentrations. This observation suggests that these metals may be removed from solution during precipitation of secondary minerals, perhaps including co-precipitation with Cr(III). Substantial increases in dissolved metal concentrations were observed in the OC experiment, including Ca (up to 17 mg L^{-1}), Fe (up to 1.9 mg L^{-1}), Mg (up to 8.8 mg L^{-1}), Na (up to 14 mg L^{-1}), and Si (up to 2.3 mg L^{-1}), along with corresponding increases in anion concentrations (Cl up to 101 mg L^{-1}, PO_4 up to 16 mg L^{-1}, SO_4 up to 29 mg L^{-1}). Benner et al. (1997) also observed a marked increase in dissolved constituents, particularly Cl, in surface water recharge that had passed through a pile of compost material used in PRB construction.

2.4.2 Chromium Removal

2.4.2.1 Aqueous Results

An initial sharp decrease in Cr(VI) concentration was observed in all batch experiments, followed by a slower removal rate until the reaction was complete (Figures 2.1 and 2.2). Measurements of Cr(VI) by spectrophotometer and Cr_{TOT} by ICP-OES and ICP-MS were in close agreement for all ZVI experiments (R^2 = 0.988-0.999), indicating that any reduced Cr(III) had been rapidly and effectively removed from solution. Similar measurements for the OC experiments were in very poor agreement, differing in concentrations by as much as 8.1 mg L^{-1} (Table 2.2). Samples from the OC experiment were strongly coloured orange-brown, even after filtering, suggesting high concentrations of DOC which may have interfered with the

spectrophotometric measurements. The highly coloured matrix did not affect Cr_{TOT} measurements, as indicated by complete recovery of a Cr-spiked OC control sample.

Removal of Cr(VI) occurred more rapidly in the single-flask ZVI-S10 than the multi-flask ZVI-M experiments, which had equivalent initial solid-solution ratios. Approximately 20% of the aqueous Cr(VI) in ZVI-S10 was removed after the first hour, progressing to almost 95% after 24 hours. In experiment ZVI-M over 50% of the Cr(VI) remained after 24 hours (Figure 2.1 and 2.2). Complete removal (< 0.1 mg L^{-1}) occurred in ZVI-M after more than 11 days. Although the two experiments initially had the same solid-solution ratio (1:25), removal of solution during sampling of ZVI-S10 changed this ratio as the experiment progressed. As the volume decreased, the remaining Cr(VI) in solution could have more easily made contact with the surface of the ZVI, increasing the rate of removal in comparison to ZVI-M. The effect of increased reaction rate was investigated by comparing single-flask experiments ZVI-S10 and ZVI-S100 (solid-solution ratio of 1:25 vs. 1:2.5). As expected, ZVI-S100 reacted much more quickly than ZVI-S10, with complete Cr(VI) removal (0.00 mg L^{-1}) observed in less than 2 hours (Figure 2.2). Accounting for the difference in mass of reactive material, the Cr(VI) removal rate of ZVI-S100 was still substantially greater per g than ZVI-S10. Increased Cr(VI) removal also was observed for the pre-treated ZVI-MP experiment in comparison to ZVI-M (same solid-solution ratio), reaching 40% removal after 1 hour and complete removal (< 0.07 mg L^{-1}) after 4.15 days (Figure 2.1). Pre-treatment of the ZVI removed the oxidized coating, exposing the Fe(II) and Fe(0) core, thus likely promoting more effective reduction of Cr(VI) from solution. In addition, BET measurements indicated that the pre-treated ZVI had a surface

area per mass ratio more than three times greater than the untreated ZVI, which may have contributed to the observed increase in Cr(VI) removal rate.

The rate of Cr(VI) removal by ZVI is dependent on Cr(VI) concentration, pH, and the surface area of Fe (Gould, 1982; Mayer et al., 2001):

(2.7) $$\frac{d[Cr(VI)]}{dt} = -k \cdot S[Cr(VI)]^{0.5}[H^+]^{0.5}$$

where $\frac{d[Cr(VI)]}{dt}$ is in units of mol L^{-1} bulk s^{-1}, k is the rate constant normalized to the ZVI surface area (L H_2O m^{-2} iron s^{-1}), S is the reactive surface area concentration of ZVI (m^2 iron L^{-1} bulk), and [Cr(VI)] and [H^+] are in units of mol L^{-1} H_2O. Rate constants were calculated for ZVI-M and ZVI-MP using measured values of Cr(VI) and pH, and the surface area measured by the Brunauer-Emmett-Teller (BET) method (Brunauer et al., 1938). The untreated ZVI had a specific surface area of 2.86±0.54 m^2 g^{-1}, whereas the surface area of the pre-treated ZVI was 9.54±0.93 m^2 g^{-1}. Calculated k values were then adjusted during geochemical modeling to fit the experimental data. Rate constants were not calculated for ZVI-S10 or ZVI-S100 because no pH measurements were conducted for these experiments due to volume restrictions. Experimental rate constant (k) values were in close agreement with values fitted in MIN3P, suggesting that the conceptual model was appropriate. The average experimental k value for ZVI-M was 7.64 x 10^{-5} L H_2O m^{-2} Fe s^{-1}, whereas the fitted value was 7.94 x 10^{-5} L H_2O m^{-2} Fe s^{-1}. Similar k values were calculated for ZVI-MP, averaging 1.73 x 10^{-4} L H_2O m^{-2} Fe s^{-1}, with a fitted value of 1.00 x 10^{-4} L H_2O m^{-2} Fe s^{-1}.

The rate of Cr(VI) removal by organic carbon is dependent on the concentration of Cr(VI) and OC (Wittbrodt and Palmer, 1995):

(2.8) $$\frac{d[Cr(VI)]}{dt} = -k[Cr(VI)][CH_2O]$$

Discrepancies between Cr(VI) and Cr_{TOT} measurements for OC-M contributed to inconsistencies in the calculated rate constants. Although the Cr(VI) data suggest that the reaction was complete after 3 days, the Cr_{TOT} value at that time was 3.7 mg L^{-1}. Using the Cr(VI) values, the overall removal rate was similar to ZVI-MP. For the purposes of geochemical modeling, the reaction was assumed to be pseudo-first order (Wittbrodt and Palmer, 1995; Tokunaga et al., 2003) and an average effective rate constant (k_{eff}) of 1.49 x 10^{-2} s^{-1} was calculated from the Cr(VI) data. Fitting of the model resulted in a k_{eff} of 1.00 x 10^{-5} s^{-1}, which was substantially different from the experimental value, suggesting that the conceptual model may not be representative of the reaction processes.

2.4.2.2 Solid-Phase Characterization

Samples at the end of each batch experiment were selected for solid-phase characterization measurements to increase the likelihood of detecting Cr-bearing precipitates. EDS mapping of several samples showed that the Cr was widely distributed across the surface of the reactive material, and a targeted collection of semi-quantitative spectra identified only minor Cr hotspots. The highest concentration of precipitated Cr was detected on ZVI-M at 8.90 wt %, though the targeted area exhibited no visual characteristics to differentiate it from the

background material (Figure 2.3b). All other ZVI samples ranged in solid-phase Cr concentration from 1.83% to 2.50% by weight. Well-developed hexagonal Fe-O-C precipitates characteristic of Fe hydroxycarbonate (Lindsay et al., 2008) were observed in the ZVI-MP samples (Figure 2.3a), but were absent from samples without exposure to $CaCO_3$ (Figure 2.3b,c). A large rhombohedral calcite crystal was observed in ZVI-MP, consistent with the carbonate precipitation suggested by the geochemical calculations (see Appendix A). Very little solid-phase Cr was detected on OC-M, a result of the same mass of Cr distributed across a much larger surface area than the ZVI samples (Figure 2.3d). Trace amounts of other elements, such as Co, Mn, Al, Ni, Si, and Mg, also were observed in all samples, with higher quantities in OC-M, which is consistent with the aqueous chemistry measurements.

XANES spectra characterized by the absence of the pre-edge 3d-4p peak indicative of Cr(VI) were observed in all samples (Figure 2.4). The Cr K-edge position the of OC-M samples was consistent with a Cr(III) oxidation state and the XANES spectra most closely resembled $Cr(OH)_3$ or Cr-acetate hydroxide. Linear combination fitting were consistent with the visual observations, suggesting that the samples contained up to 20% Cr-acetate and balance $Cr(OH)_3$ (Table 2.2).

Although the dominant Cr K-edge position of the ZVI-M samples also was consistent with a Cr(III) oxidation state, a small shoulder was observed on some spectra in the same position as Cr metal (Figure 2.4). The presence of up to 37% Cr metal was suggested by linear combination fitting, whereas ZVI-M samples without the observed shoulder generally were > 85% $Cr(OH)_3$. Chemical analysis revealed that Connelly ZVI contains up to 0.2 wt % Cr (Connelly GPM, written communication). Under a bulk X-ray beam, both elemental Cr metal

in the reactive material and precipitated Cr(III) would be represented in the sample spectra, resulting in the occasional appearance of a Cr metal shoulder similar to that observed in Figure 2.4. The complete absence of the characteristic Cr(VI) pre-edge feature demonstrates the reduction of Cr(VI) to Cr(III) for all reactive materials. Results from XPS analysis further support reduction to a Cr(III) oxidation state. Fitting of the Cr 2p spectra suggests that the dominant form is $Cr(OH)_3$ for both ZVI-M and ZVI-MP. No Cr was detected on OC-M samples during XPS analysis, likely due to the small mass of Cr distributed over a large surface area.

2.4.3 Chromium Isotope Fractionation

2.4.3.1 Influence of Material

The reactivity of untreated and pre-treated ZVI was compared with the ZVI-M and ZVI-MP experiments, which differed only in preparation of the reactive material. Isotopic composition of the input solutions exhibited $\delta^{53}Cr$ values of 0.00±0.08‰ for ZVI-M and 0.07±0.10‰ for ZVI-GW relative to SRM 979. Decreasing Cr(VI) concentrations were accompanied by an increase in $\delta^{53}Cr$ values up to 1.85±0.10‰ relative to the input for ZVI-M and 1.30±0.09‰ for ZVI-MP (Figure 2.5). Isotopic data were fitted to a Rayleigh-type fractionation curve generating α values of 0.9994 and 0.9995, suggesting that the degree of fractionation was very small.

Reduction of Cr(VI) by ZVI is thought to occur via two possible mechanisms: (1) heterogeneous (direct) reduction by contact with the ZVI surface following adsorption of Cr(VI), and (2) homogeneous (indirect) reduction by dissolved Fe(II) released during

heterogeneous reduction (Gheju, 2011). Sorption of aqueous Cr(VI) does not cause significant isotope fractionation (α = 1.0000), since no change in coordination occurs (Ellis et al., 2004; Schauble et al., 2004). In contrast, for homogeneous reduction (i.e. reduction in solution) Ellis et al. (2002) established a fractionation factor of 0.9965, a value that also was observed by Døssing et al. (2011). The isotope results for both ZVI-M and ZVI-MP suggest Cr(VI) removal was dominated by sorption. Subsequent reduction to Cr(III) on the ZVI surface, as indicated by solid-phase analysis, would have no effect on the isotopic composition of the remaining Cr(VI) in solution. Assuming α = 1.0000 for sorption and α = 0.9965 for reduction in solution, a calculation was performed similar to Døssing et al. (2011) to determine the proportion of Cr(VI) removal attributed to each mechanism. Using an average α = 0.9994 for ZVI-M and ZVI-MP, the results from this calculation indicate that 83% of Cr(VI) removal by ZVI was the result of direct reduction following sorption, whereas only 17% was the result of homogeneous reduction in solution.

The Cr isotope measurements indicated that the mechanism was similar for both untreated and pre-treated ZVI experiments. These results, coupled with the solid-phase analyses, suggest that sorption followed by reduction at the ZVI surface was the dominant Cr(VI) reduction mechanism for Connelly ZVI. Slower removal rates in ZVI-M may be indicative of the greater time required for the Cr(VI) to penetrate the oxidation layers and reach the Fe(II) and Fe(0) core needed for reduction (Gheju, 2011).

2.4.3.2 Influence of Experimental Design

Single- and multi-flask batch experiment designs were compared with ZVI-S10 and ZVI-M, which initially contained the same solid-solution ratio. The Cr in the input solution for ZVI-S10 had a δ^{53}Cr value of -0.03±0.09‰. An increase in δ^{53}Cr up to 2.01±0.13‰ relative to the input solution (Figure 2.5) was observed, corresponding to a steady decrease in Cr(VI) concentration. Data from ZVI-S10 was fitted to a Rayleigh-type curve, and the calculated $\alpha = 0.9993$ was nearly identical to the $\alpha = 0.9994$ calculated for ZVI-M.

The comparison between the single-flask batch experiment and the multi-batch experiment was made to evaluate whether changing solid-solution ratios as samples were gathered through the experiment would artificially enhance the isotope fractionation. An analogous multi-flask experiment should not induce an artificial enhancement because a separate bottle is used for each sample in the time series. A significant increase in reaction rate was observed in ZVI-S10, which reached completion after 3 days, while ZVI-M was complete after 11 days. This increased reaction rate was likely due to the changing solid-solution ratio in ZVI-S10; as the volume of solution decreased, the mass of Cr(VI) in the remaining volume would have been in greater contact with the surface of the reactive material. Nonetheless, the isotope measurements provided a fractionation factor for ZVI-S10 that was nearly identical to the value obtained for ZVI-M, indicating no effect from the diminishing reservoir volume in the single-flask experiment. These results also demonstrate that the mechanism of Cr(VI) removal was the same in both experiments, despite the difference in reaction rate.

2.4.3.3 Influence of Reaction Rate

The rate of Cr(VI) removal was increased by adjusting the mass of ZVI from 10 g in ZVI-S10 to 100 g in ZVI-S100, while maintaining identical initial solution volumes. The reaction in ZVI-S100 progressed to completion in less than 2 hours, while exhibiting isotope fractionation that increased from the initial $\delta^{53}Cr = -0.03 \pm 0.09‰$ to $\delta^{53}Cr = 2.29 \pm 0.13‰$ relative to the input (Figure 2.5). Fitting the isotope data from ZVI-S100 to a Rayleigh-type curve generated a fractionation factor of 0.9994, nearly identical to the $\alpha = 0.9993$ for ZVI-S10. These results suggest that a change in reaction rate due to a change in the mass of reactive material did not have an effect on the extent of isotope fractionation. Fractionation is expressed as the ratio of the individual isotope reaction rates (Clark and Fritz, 1997), so it follows that the isotope fractionation should not change as the overall reaction rate changes.

2.4.3.4 Organic Carbon Results

Unlike the ZVI batch experiments, results of the organic carbon repeat experiments (OC-MA and OC-MB) differed substantially, likely due to a change in shaking technique between the two sets of experiments. Concentrations of Cr(VI) in the OC-MB batch declined to 0.04 mg L^{-1} after 3 days, while the concentrations in the OC-MA batch declined to less than 50% of the initial Cr(VI) after the same period (Table 2.2). The results were further complicated by a significant difference between Cr(VI) and Cr_{TOT} concentrations. As discussed in Section 2.4.2.1, Cr_{TOT} measurement accuracy was demonstrated by spiking the DOC-rich matrix with a known quantity of Cr standard. Initial observations thus suggest that the Cr(VI) measurements

by Hach spectrophotometer were erroneous, perhaps due to the strong orange-brown colour of the solution.

A δ^{53}Cr value of -0.05±0.09‰ was observed for the input solution of OC-MA, while a value of 0.01±0.09‰ was observed for OC-MB. As expected, the majority of OC-M samples exhibited an increase in δ^{53}Cr with decreasing Cr(VI) concentration (Table 2.2). This trend ceased for the last sample of OC-MA, collected at 24 days after the start of the experiment. Although Cr(VI) measurements suggested that the reaction was complete, Cr_{TOT} analysis by ICP-OES indicated that 8.3 mg L^{-1} Cr remained in solution. Isotope analysis revealed a δ^{53}Cr value of -0.45±0.10‰, corroborated by duplicate sample aliquots that were processed and analyzed independently.

Application of Cr isotopes for tracking Cr(VI) in groundwater assumes that all reduced Cr(III) is rapidly and completely removed from solution, usually through precipitation, which should occur readily at the circumneutral to high pH values observed in the OC-M batch experiments (Blowes, 2002). Rayleigh-type isotope fractionation relies on complete isolation of the product from the reactant, causing an exponential increase in positive δ^{53}Cr values in the remaining Cr(VI) pool, and corresponding negative δ^{53}Cr values in the reacted Cr(III) (Ellis et al., 2002). A negative δ^{53}Cr value thus suggests that the Cr(VI) was not completely isolated from the reacted Cr(III). The sample preparation procedure described in Section 2.3.3 assumed that only Cr(VI) is present in solution, which is valid if the Cr(VI) and Cr_{TOT} data can be closely correlated. If both unreacted Cr(VI) and reduced Cr(III) co-existed simultaneously in solution, the resulting Cr isotope analysis would be an average of the positive δ^{53}Cr of the

Cr(VI) and the negative δ^{53}Cr of the Cr(III). The overall δ^{53}Cr may either be negative or positive, according to the proportion of mass contributed from each oxidation state.

Although the majority of the δ^{53}Cr values for both OC-MA and OC-MB were positive, the observation of a negative value for only one sample suggested that all of the results required further examination. The Cr isotope results for the OC experiments potentially represented a contribution from both Cr(VI) and Cr(III). Despite filtering the solution first at 0.45 μm during vacuum-filtering and then at 0.2 μm during subsampling, it appeared that the samples retained for analysis contained Cr(III). Precipitated Cr would have been removed during filtering, suggesting that dissolved Cr(III) remained in the solution, perhaps complexed with DOC. As a result, it was not possible to characterize the fractionation curve for the OC-M batch experiments using samples processed in the manner outline in Section 2.3.3. Further development of the sample preparation procedure would be required to separate the Cr(VI) and Cr(III) in solution prior to isotope analysis. Evidence of unprecipitated Cr(III) indicated that more testing is necessary to fully understand the mechanism of Cr(VI) removal by organic carbon, and to characterize the associated Cr isotope fractionation.

2.4.4 Implications for Tracking Cr(VI) in Groundwater

Understanding the dominant removal mechanism in a given environment is crucial for the application of Cr isotopes for tracking Cr(VI) migration in groundwater. Batch experiments to evaluate the influence of Cr(VI) removal on isotope fractionation are necessary prior to interpretation of field samples. Results from all ZVI batch experiments suggested that the dominant mechanism for Cr(VI) treatment by Connelly ZVI was heterogeneous reduction.

Characterized by a primary sorption step (Gheju, 2011), this mechanism resulted in little isotopic fractionation in the remaining Cr(VI) pool. In the case of a permeable reactive barrier (PRB) composed of Connelly ZVI, a lack of substantial Cr isotope fractionation may not necessarily be indicative of a lack of treatment by reduction. This study showed that although the extent of isotope fractionation during Cr(VI) treatment by ZVI was relatively small, solid-phase analysis indicated reduction to Cr(III), which is the desired effect of this type of groundwater treatment (Blowes et al., 2000).

Experiments designed to evaluate Cr(VI) reduction using untreated ZVI are likely most representative of the condition of ZVI immediately following the construction of a PRB. Once below ground, however, reducing conditions develop naturally as the ZVI is exposed to low-oxygen, $CaCO_3$-saturated groundwater of the Cr(VI) plume (Mayer et al., 2001). Comparison experiments in this study demonstrated that although the removal rates were much more rapid for the pre-treated ZVI, the dominant Cr(VI) reduction mechanism was the same for untreated and pre-treated ZVI, exhibiting indistinguishable isotope fractionation curves. Indications that the reaction rate had no effect on the Cr isotope fractionation, provided the mechanism of removal remains unchanged, simplifies the use of Cr isotopes for assessing treatment of Cr(VI)-contaminated groundwater.

2.5 Conclusions

- Treatment of Cr(VI) by Connelly ZVI was accompanied by a slight Cr isotope fractionation, exhibiting a Rayleigh-type curve with a corresponding average $\alpha = 0.9994$.

- Isotope results indicated that removal of Cr(VI) by Connelly ZVI was dominated by a heterogeneous reduction mechanism, which is characterized by sorption prior to reduction.
- Pre-treatment of ZVI to remove oxidized coatings improved Cr(VI) removal rates but had no effect on Cr isotope fractionation, suggesting that the removal mechanism was the same as removal by the untreated ZVI.
- Experimental design had no effect on the isotope results in this study. A multi-flask design is preferable because it allows solid analysis to be conducted over time, whereas solid analysis in a single-flask design is only possible at the conclusion of the experiment.
- Changes in reaction rate by adjusting the mass of reactive material had no effect on Cr isotope fractionation, simplifying the application of this tool to field settings.
- Isotope analysis of OC experiments resulted in a negative δ^{53}Cr value, suggesting that Cr(III) remained in solution, possibly complexed with DOC. Further research is required to understand the Cr(VI) removal mechanism by organic carbon, and to separate the Cr(VI) from Cr(III) prior to isotope analysis.
- Simple and careful batch experiments such as those performed in this study are essential to identify the mechanism of Cr(VI) reduction and characterize the associated isotope fractionation. Batch experiments should be performed with various reactive materials, and under various conditions, prior to the application of Cr isotopes as a tool to track Cr(VI) migration in groundwater.

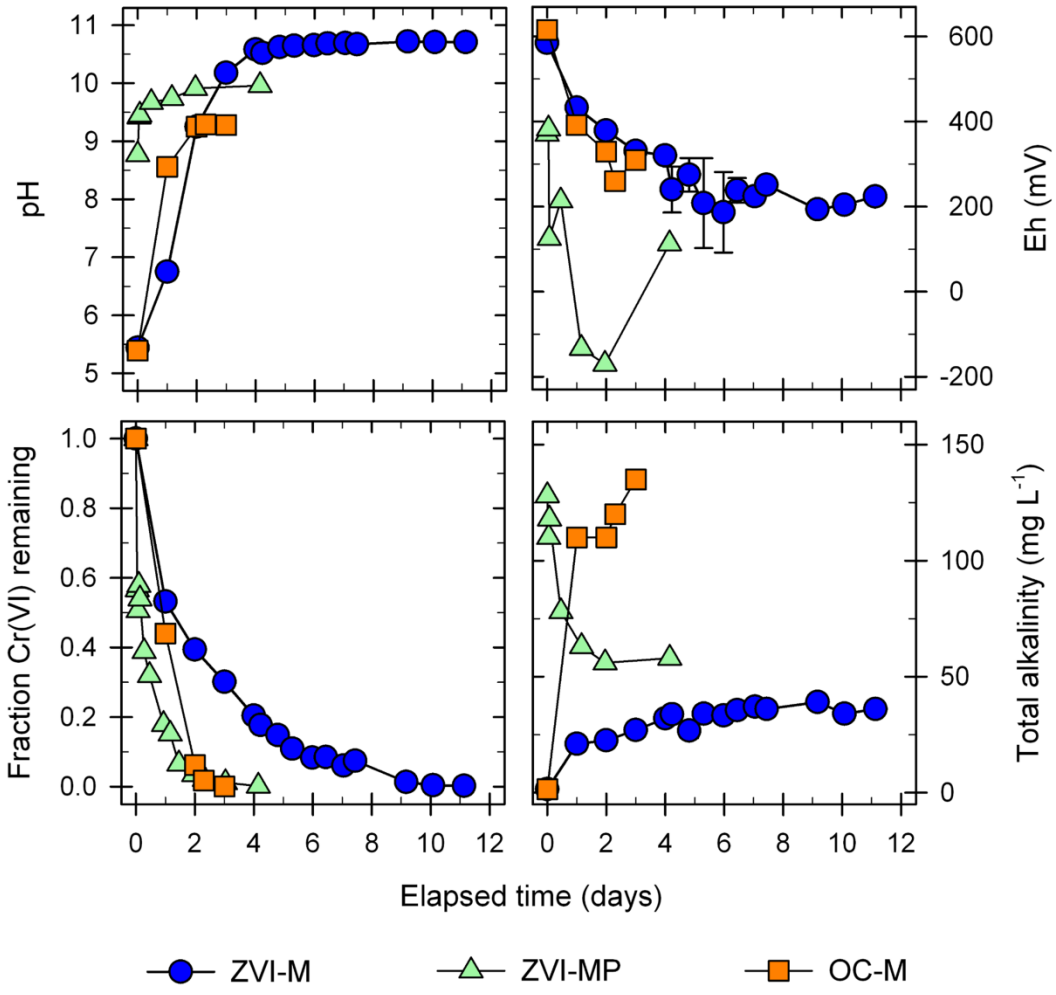

Figure 2.1 Aqueous geochemistry as a function of time for multi-flask batch experiments. Error bars represent standard deviation of replicate samples within the time series (error bars are smaller than symbols for some analyses; see Appendix A for list of replicate samples). Total alkalinity is expressed as mg L^{-1} $CaCO_3$. Fraction of Cr(VI) remaining was calculated as C/C_0 using Cr_{TOT} values for ZVI-M and ZVI-MP and Cr(VI) values for OC-M.

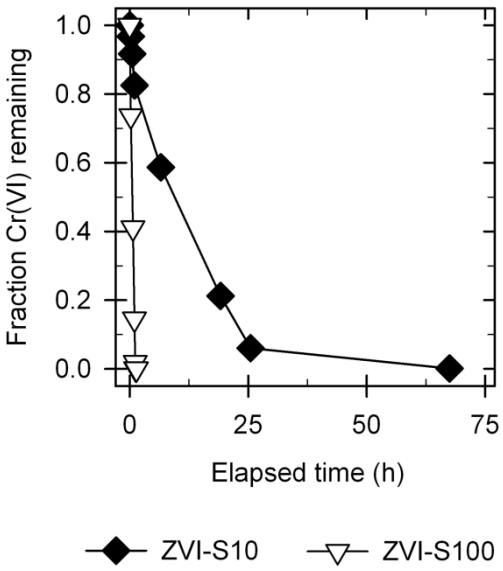

Figure 2.2 Fraction of Cr(VI) remaining in solution as a function of time for the single-flask batch experiments.

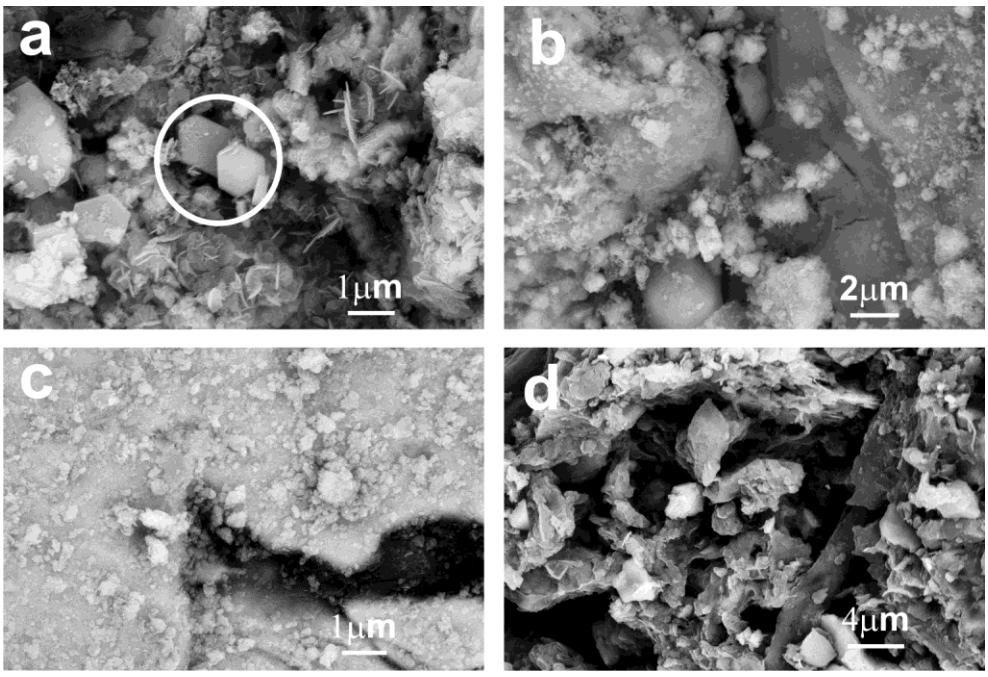

Figure 2.3 Backscatter SEM images for (a) ZVI-MP, (b) ZVI-M, (c) ZVI-S100, and (d) OC-M. All samples were taken from the end of each experiment. Circle in (a) indicates hexagonal Fe-O-C precipitates characteristic of Fe hydroxycarbonate.

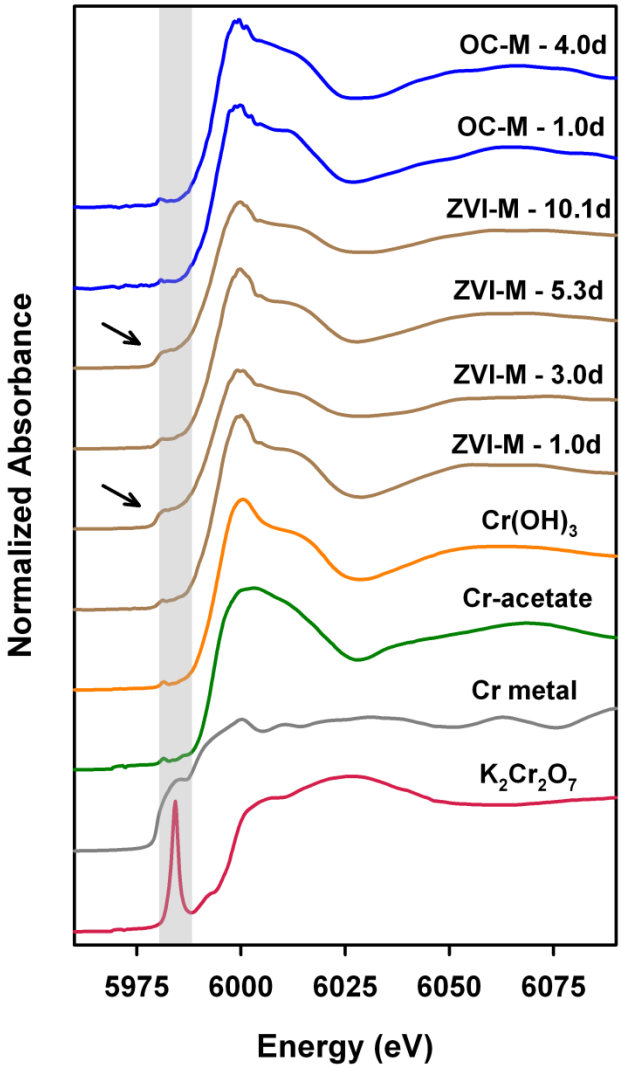

Figure 2.4 Bulk XANES spectra of Cr for a selection of ZVI and OC samples. Reference materials represent three Cr oxidation states: Cr(III) as $Cr(OH)_3$ and Cr-acetate hydroxide, Cr(0) as Cr metal, and Cr(VI) as $K_2Cr_2O_7$. Shaded area indicates peak position for Cr(VI). Arrows indicate the small shoulder observed on certain ZVI samples, likely from the Cr metal content of the reactive material.

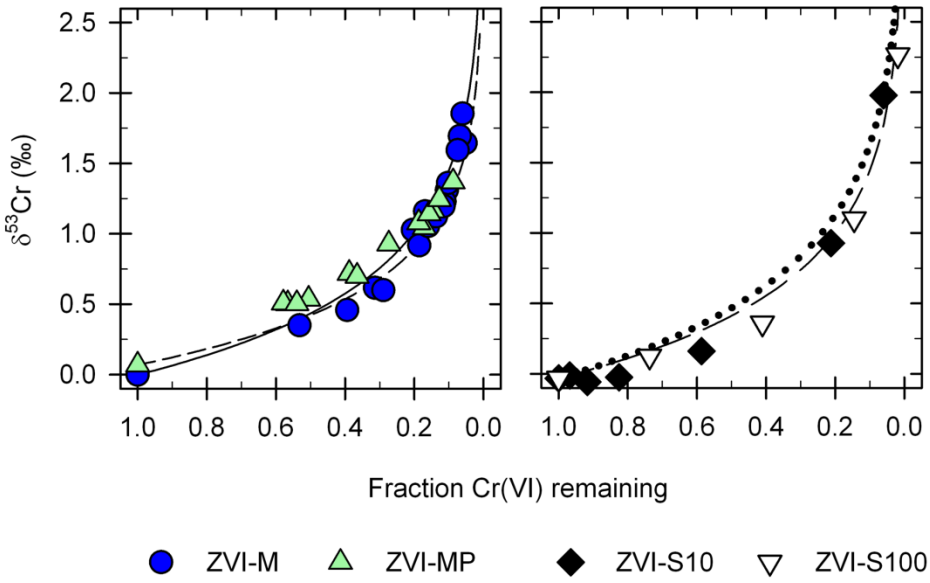

Figure 2.5 Isotope results for all ZVI batch experiments. Rayleigh-type fractionation was observed for all experiments, generating very similar fractionation factors as follows: ZVI-M α = 0.9994 (solid line), ZVI-MP α = 0.9995 (short-dashed line), ZVI-S10 α = 0.9993 (dotted line), and ZVI-S100 α = 0.9994 (long-dashed line).

Table 2.1 Summary of type of reactive material and experimental conditions for batch experiments.

Experiment	Type	Reactive material	Mass solids (g dry wt)	Input volume (mL)	Input matrix
ZVI-S10	single	Connelly ZVI	10	250	DI water
ZVI-S100	single	Connelly ZVI	100	250	DI water
ZVI-M	multi	Connelly ZVI	6	150	DI water
ZVI-MP	multi	Connelly ZVI, pre-treated	6	150	$CaCO_3$-saturated DI water
OC-M	multi	leaf mulch	6	150	DI water

Table 2.2 Summary of results from replicate organic carbon batch experiments. An orbital shaker was used for OC-MA, while hand-shaking was implemented for OC-MB.

Experiment	Time (days)	Concentration (mg L^{-1})		$\delta^{53}Cr$ (‰)	±1σ (‰)
		Cr(VI)	Cr_{TOT}		
OC-MA	0.00	51	49.1	-0.05	0.09
	0.09	40	34.5	0.14	0.09
	0.93	32	28.9	0.45	0.09
	1.75	35	30.6	0.27	0.09
	4.75	25	21.2	0.53	0.08
	24.0	0.20	8.3	-0.45	0.10
OC-MB	0.00	50	46.1	0.01	0.09
	1.00	22	16.8	0.61	0.08
	2.00	3.1	9.8	0.86	0.09
	2.30	0.90	4.9	1.03	0.09
	3.00	0.04	3.7	n/a	n/a

n/a = Cr concentration too low for isotope analysis

Table 2.3 Linear combination fitting results for XANES analysis on ZVI-M and OC-M samples. Standards used for ZVI-M fitting included $Cr(OH)_3$ and Cr metal; Cr-acetate was added for OC-M fitting.

Experiment	Time (days)	Content (%)		
		$Cr(OH)_3$	Cr metal	Cr-acetate
ZVI-M	1.00	94.7	5.3	-
	2.00	98.0	2.0	-
	3.00	63.4	36.6	-
	4.00	88.0	12.0	-
	4.81	77.2	22.8	-
	5.31	85.1	14.9	-
	7.04	92.3	7.7	-
	10.08	68.7	31.3	-
	11.13	89.0	11.0	-
OC-M	1.00	76.1	5.1	18.9
	2.00	74.4	6.0	19.6
	3.00	76.6	3.4	20.0

Chapter 3:

Chromium Isotope Fractionation During Reduction of Cr(VI) Under Saturated Flow Conditions

3.1 Summary

Chromium isotopes are promising indicators of Cr(VI) reduction in groundwater; however, the influence of transport on fractionation has not been fully examined. A laboratory column experiment was conducted to evaluate isotopic fractionation of Cr during Cr(VI) reduction under controlled flow conditions. Simulated groundwater containing 20 mg L^{-1} Cr(VI) was pumped through a saturated column containing quartz sand with 10% (v/v) organic carbon. Isotope measurements were performed on both effluent and profile samples. Dissolved Cr(VI) concentrations decreased while δ^{53}Cr increased, indicating that reduction of Cr(VI) occurred. Solid-phase analysis by scanning electron microscopy (SEM) and X-ray absorption near edge structure (XANES) spectroscopy indicated the presence of Cr(III) on the surface of the organic carbon. The δ^{53}Cr data followed a linear regression equation yielding a fractionation factor (α) of 0.9979, whereas previous studies of batch experiments under similar geochemical conditions demonstrated Rayleigh-type isotope fractionation. The linear characteristic of the current δ^{53}Cr data may reflect the contribution of transport on Cr isotope fractionation.

3.2 Introduction

Hexavalent chromium (Cr(VI)) is a pervasive groundwater contaminant, frequently derived from industrial activities such as tanning and electroplating (Blowes, 2002). This toxic and carcinogenic contaminant Cr(VI) is highly soluble and mobile in groundwater as $HCrO_4^-$, CrO_4^{2-} and $Cr_2O_7^{2-}$ oxyanions (Losi et al., 1994). The reduction of Cr(VI) to Cr(III), which is characterized by low solubility in groundwater, decreases Cr mobility (Palmer and Wittbrodt,

1991). Therefore, the mobility of Cr in groundwater is controlled by the availability of electron donors that promote Cr(VI) reduction.

There are four stable Cr isotopes, ^{50}Cr, ^{52}Cr, ^{53}Cr, and ^{54}Cr, with natural abundances of 4.35%, 83.8%, 9.5%, and 2.37%. Various mechanisms can cause a shift in the $^{53}Cr/^{52}Cr$ ratio, the most important of which are redox changes due to the transition from tetrahedrally-coordinated Cr(VI) to octahedrally-coordinated Cr(III) (Schauble et al., 2004). Materials known to effectively reduce Cr(VI) include Fe(II) (Eary and Rai, 1988; Ellis et al., 2002), zero-valent iron (Blowes et al., 1997; Jeen et al., 2008), organic carbon (Bolan et al., 2003; Park et al., 2008), and certain bacteria (Cummings et al., 2006; Sikora et al., 2008). Preferential reaction of the lighter isotopes during reduction results in an enrichment in ^{53}Cr relative to ^{52}Cr in the remaining Cr(VI) pool. The application of stable Cr isotope ratios to groundwater has been proposed as a method to track Cr(VI) migration processes (Blowes, 2002; Ellis et al., 2002). Although measurements of Cr(VI) concentrations provide limited information on the conditions of the subsurface environment, shifts in $\delta^{53}Cr$ values are indicative of mass-transfer processes (Losi et al., 1994; Blowes, 2002). Laboratory batch experiments have demonstrated that the degree of isotope enrichment is dependent on the mechanism of removal and the reductant (Ellis et al., 2002, 2004; Sikora et al., 2008; Berna et al., 2010; Zink et al., 2010; Døssing et al., 2011). Increases in $\delta^{53}Cr$ values have been observed in field settings (Ellis et al., 2002; Izbicki et al., 2008; Berna et al., 2010; Raddatz et al., 2011), though relationships between Cr(VI) concentrations and $^{53}Cr/^{52}Cr$ ratios often are found to be complicated by system heterogeneity and natural background concentrations (Izbicki et al., 2008; Berna et al., 2010).

The application of Cr stable isotopes to track Cr(VI) migration in groundwater relies upon a detailed understanding of relationships between $\delta^{53}Cr$ values and the processes that control Cr mobility. The influence of transport on isotope fractionation during Cr(VI) reduction is largely unknown. Ellis et al. (2004) predicted that the $\delta^{53}Cr$ signature may be skewed at the fringes of a plume due to magnification of the very slight fractionation that could occur due to sorption of Cr(VI). In this study, a laboratory column experiment was conducted to evaluate Cr(VI) reduction by organic carbon under saturated flow conditions. Analyses of the stable Cr isotope ratios, water chemistry, and solid-phase geochemistry were performed, providing results to assess the influence of transport on Cr isotope fractionation.

3.3 Materials and Methods

3.3.1 Experimental Setup

Simulated groundwater containing 20 mg L^{-1} Cr(VI) was prepared by dissolving $K_2Cr_2O_7$ in $CaCO_3$-saturated deionized water. This solution was pumped in an upward direction through a 40 cm long column packed with 90% (v/v) quartz sand and 10% (v/v) organic carbon as mixed deciduous-tree leaf mulch from a local landfill. The column had an inner diameter of 5 cm, was fitted with influent and effluent ports, and had 15 sampling ports positioned at 2.5 cm intervals along its length. A flow rate of approximately 0.35 pore volumes (PVs) per day was employed. Effluent samples were collected at 3 to 4 day intervals, and measurements of pH, redox potential (Eh relative to the standard hydrogen electrode) and alkalinity were made. The pH was determined using an Orion Ross 815600 electrode (Thermo Scientific, Waltham, MA), which was calibrated with standard pH 4 and 7 buffers. The Eh electrode (Orion 9678, Thermo

Scientific) was tested with Zobell's solution (Nordstrom, 1977) and Light's solution (Light, 1972) prior to sampling. Sub-samples were passed through 0.45 μm Supor membrane filters (Acrodisc, Pall, UK) and retained for anion, cation and Cr isotope analyses. Alkalinity measurements were performed on filtered sample aliquots by adding the bromocresol green-methyl red indicator and titrating to the end point with H_2SO_4. Two sets of profile samples also were collected after approximately 5.5 and 8.5 PVs. Concentrations of Cr(VI) were initially measured on a Hach DR/2010 spectrophotometer at 540 nm using the 1,5-diphenylcarbohydrazide method (Greenberg et al., 1992). Concentrations of inorganic anions were determined by ion chromatography (Dionex DX 600). Cation concentrations were measured by inductively-coupled plasma mass spectrometry (Thermo Scientific XSeries 2) on samples acidified to pH < 2 with trace-metal grade HNO_3.

3.3.2 Isotope Measurements

Acidified samples were purified and pre-concentrated for Cr isotope analysis using an ion-exchange separation method modified from Ball and Bassett (2000). All sample preparations were carried out in a HEPA-filtered laminar flow hood. Sample aliquots were mixed at a known ratio with a ^{50}Cr-^{54}Cr double spike solution composed of enriched Cr metal (ISOFLEX USA, San Francisco, CA) dissolved in 2 N HNO_3. The mixture was gently boiled with 0.2 mol L^{-1} ammonium persulfate for ~25 minutes to oxidize the Cr (Schoenberg et al., 2008). A 3 mL SPE column was loaded with 0.5 mL Bio Rad AG1-X8 anion exchange resin sandwiched between two 20 μm frits. The resin was conditioned by sequentially passing through 2 mL each of 6 N, 4 N, 2 N, and 1 N HNO_3, followed by 20 mL of high-purity Milli-Q® water. Oxidized

sample-spike mixtures were pipetted onto the exchange resin and flushed with 15 mL of water to remove impurities. The Cr(VI) retained on the exchange resin was reduced to Cr(III) by saturating the resin in 2 N HNO_3 for 2 hours. After reduction the Cr was eluted into the sample vial with 2 N HNO_3 and Milli-Q®, then diluted to achieve a final concentration of 1-2 mg L^{-1} Cr.

High-precision Cr isotope measurements were performed by multi-collector inductively-coupled plasma mass spectrometry (Thermo Scientific Neptune) in medium-resolution mode using the stable inlet system (double cyclonic spray chamber). All four stable Cr isotopes (^{50}Cr, ^{52}Cr, ^{53}Cr, and ^{54}Cr) were measured simultaneously along with ^{49}Ti, ^{51}V, and ^{56}Fe to facilitate corrections due to isobaric interferences on ^{50}Cr and ^{54}Cr. Off-centre peak measurements were performed to minimize polyatomic interferences from $^{40}Ar^{14}N$ on ^{54}Cr and $^{40}Ar^{16}O$ on ^{56}Fe. Sensitivity on the ^{52}Cr signal was in the range of 4-6 V ppm^{-1}. Integration time was 4.194 seconds, with 1 block of 100 cycles.

The ^{50}Cr-^{54}Cr double spike solution was used to quantify isotope fractionation induced by sample preparation and instrumental mass bias. A double-nested iterative routine was implemented to subtract the contribution from Ti, V, and Fe, and extract the composition of the naturally fractionated sample (Siebert et al., 2001). A 2σ outlier test was performed on the raw data, after which the iterative routine was applied to each of the individual measurements, averaging only the final values. The results are expressed as $\delta^{53}Cr$ in per mil (‰) relative to the NIST SRM 979 Cr isotope standard, where:

(3.1) $$\delta^{53}Cr = \left[\frac{\left(^{53}Cr/^{52}Cr\right)_{sample} - \left(^{53}Cr/^{52}Cr\right)_{standard}}{\left(^{53}Cr/^{52}Cr\right)_{standard}}\right] \times 1000$$

External reproducibility for this method was calculated to be ±0.1‰ (2σ) on the $^{53}Cr/^{52}Cr$ ratio, determined from daily measurements of SRM 979 prepared with each sample set. Submission of four unknown samples to an independent laboratory for Cr isotope analysis validated the performance of the above method within ±0.06‰ (2σ).

3.3.3 Solid-Phase Cr Characterization

Samples of column solids were collected, frozen, and freeze-dried prior to solid-phase analysis. Field emission-scanning electron microscopy (FE-SEM; Leo1530, Carl Zeiss SMT GmbH, Germany) with energy dispersive spectroscopy (EDS; EDAX Pegasus 1200, AMETEK Inc., USA) were used to examine secondary precipitates. The dried samples were mounted on Al stubs with C tape and coated with a 10-12 nm thick Au layer to ensure conductance. An accelerating potential of 20 kV was used for backscatter electron (BSE) imaging and collection of semi-quantitative EDS spectra.

Synchrotron-based X-ray fluorescence (XRF) and X-ray absorption near edge structure (XANES) spectroscopy were performed at the GSE-CARS beamline 13-BM-D at the Advanced Photon Source, Argonne National Laboratory (Chicago, IL). Organic carbon and sand particles were mounted separately in 1 mm-thick Al sample holders between two layers of Kapton® tape. Reference materials were ground using an acid-washed agate mortar and pestle and passed through a 63 μm stainless steel sieve. These materials were spread onto

polyethylene terephthalate (PET) tape (Scotch Magic Tape, 3M, St. Paul, MN), which was layered to a thickness of 300 - 500 μm and sealed between two additional layers of PET tape. Bulk Cr K-edge XANES spectra were collected with an unfocused incident beam (~0.5 × 3 mm). Spectra for samples were collected using a four-element Si detector (Vortex ME-4, SII NanoTechnology USA Inc., Northridge, CA), whereas spectra for reference materials were collected in transmission mode. Processing of XANES data was performed using the program ATHENA, which is a component of the IFEFFIT software package (Ravel and Newville, 2005).

3.4 Results and Discussion

3.4.1 Effluent Chemistry

Effluent pH values ranged from 6.70 to 8.04, averaging 7.16±0.71 over the course of the experiment. Redox potential varied over time, ranging from approximately 400 mV to nearly 600 mV. Alkalinity in the effluent initially was 600 mg L^{-1} (as $CaCO_3$) and exhibited a steady decrease to < 100 mg L^{-1} after complete Cr breakthrough. Effluent calcium concentrations were initially 250 mg L^{-1}, decreasing to 50 mg L^{-1} following complete breakthrough.

3.4.2 Chromium Removal

Decreases in aqueous Cr(VI) concentrations were observed in the column, and complete Cr(VI) removal was observed during the first 2 PVs of flow. After this time, effluent Cr(VI) concentrations began to increase and complete breakthrough was observed after ~12 PVs (Figure 3.1). Between 2 and 12 PVs, the effluent concentration of Cr(VI) increased slowly to

the input value of 20 mg L^{-1}. Both sets of profile samples, collected after 5.5 and 8.5 PVs, captured the progression of the Cr(VI) concentration front through the column. The front progressed ~10 cm further in the second profile (Figure 3.2), demonstrating a large decrease in organic carbon reactivity in the first half of the column, where the Cr(VI) concentrations remained at the input concentration.

Discrete Cr-bearing precipitates were observed on organic carbon particles collected at the conclusion of the experiment (Figure 3.3). Similar precipitates were not observed in the initial organic carbon material. In addition to Cr, these precipitates commonly contained Fe and Ni. Atomic ratios of Fe:Cr ranged from 3.6 to 4.1, whereas Ni:Cr ratios of 0.40 to 0.45 were observed. Though the chemical composition of the Cr-bearing precipitates was relatively consistent, their morphology varied both within and among the samples. The occurrence of Cr with other metals suggests that co-precipitation reactions contributed to Cr removal. Additionally, other metal-bearing phases may have served as nucleation sites for the formation of Cr-bearing precipitates.

Preliminary XRF spectra were collected independently for both sand and organic carbon particles. Chromium was not detected on the sand particles; therefore, XANES analysis was not performed on this material. Spectra collected for organic carbon samples were consistently characterized by the absence of the pre-edge 3d-4p peak that is characteristic of Cr(VI) (Figure 3.3). All column samples exhibited similar XANES spectra. The Cr K-edge positions were consistent with a Cr(III) oxidation state and the XANES spectra closely resemble $Cr(OH)_3$ or Cr-acetate hydroxide. The presence of Cr(III) and the general lack of Cr(VI) on the organic carbon particles were indicative of in situ Cr(VI) reduction.

The removal of aqueous Cr(VI) by organic carbon is thought to occur via two possible mechanisms: Mechanism I involves direct reduction of Cr(VI) in solution, whereas Mechanism II incorporates sorption of Cr(VI) with organic carbon, followed by reduction to Cr(III) and either release or complexation (Park et al., 2005; Park et al., 2007). If the Cr(VI) removal mechanism was due simply to reduction in the bulk solution followed by Cr(III) precipitation, $Cr(OH)_3$ may be expected to occur on both the sand and the organic carbon particles. The apparent absence of Cr on sand particles suggests that Cr(VI) reduction in solution was localized around organic carbon particles, followed rapidly by precipitation of $Cr(OH)_3$ due to the circumneutral pH (Rai et al., 1987). Sorption of Cr(VI) must also be followed by rapid reduction and precipitation of $Cr(OH)_3$, as indicated by the lack of the characteristic Cr(VI) pre-edge peak on the XANES spectra.

3.4.3 Chromium Isotope Fractionation

The input solution averaged a $\delta^{53}Cr$ value of -0.01±0.06‰, relative to SRM 979. Decreases in Cr(VI) concentrations were accompanied by increases in the $\delta^{53}Cr$ values of up to 2.00±0.10‰ relative to the input solution (Figures 3.1&3.2). This trend was observed in both sets of profile samples and the effluent.

Isotope fractionation curves for Cr reduction generally have been fitted to a Rayleigh distillation model (Ellis et al., 2002; Sikora et al., 2008; Berna et al., 2010; Zink et al., 2010; Døssing et al., 2011). This model assumes a closed system in which the reduced Cr(III) is isolated from the remaining Cr(VI), such as by precipitation, and no back-reaction occurs. As the proportion of reduced Cr(III) increases, the pool of Cr(VI) becomes exponentially more

enriched in the heavy isotopes. Data from this column experiment initially were fitted to a Rayleigh fractionation curve, but this model did not describe the observed data (Figure 3.4). A linear regression of δ^{53}Cr vs. the fraction of Cr(VI) remaining in solution (f) provides the best fit to the experimental data (R^2 = 0.925). The fractionation factor, α, was then calculated from the linear regression:

(3.2) $$\Delta^{53/52}Cr = \delta^{53}Cr_{initial} - \delta^{53}Cr_{f=0} = 1000 \times \ln \alpha$$

where $\delta^{53}Cr_{initial}$ is the average value of the input solution and $\delta^{53}Cr_{f=0}$ is obtained from the y-intercept of the regression line when no Cr(VI) remains (f = 0).

Only one study has reported Cr isotope results that are not fitted to a Rayleigh fractionation model. During Cr(VI) reduction by H_2O_2 under acidic conditions, Zink et al. (2010) observed an isotope fractionation that exhibited an equilibrium effect with a $\Delta^{53/52}Cr_{(Cr(III)-Cr(VI))}$ value of -3.54‰ (where $\Delta^{53/52}Cr_{(Cr(III)-Cr(VI))} \approx 10^3$ x lnα, or α = 0.9965). At circumneutral pH, a kinetic effect was observed with a $\Delta^{53/52}Cr_{(Cr(III)-Cr(VI))}$ value of -5.0‰ (α = 0.9950). The equilibrium behaviour at very low pH was attributed to first-order reduction, which occurs only under highly acidic conditions. A lack of intermediate Cr(V) or Cr(IV) species during reduction from Cr(VI) to Cr(III) likely contributed to the absence of the kinetic effect.

The pH in the column was near neutral throughout the current study, so it is unlikely that equilibrium behaviour under acidic conditions observed by Zink et al. (2010) is relevant to

this system. Fitting a Rayleigh curve to the isotope data assumes a closed system. Unlike the batch experiments carried out in previous studies (Ellis et al., 2002; Sikora et al., 2008; Berna et al., 2010; Zink et al., 2010; Døssing et al., 2011), a column is not a closed system. Instead, a constant source of Cr(VI) is introduced to the column, with a uniform concentration and isotopic composition. As the Cr(VI) in the column undergoes fractionation due to reduction, the isotopically enriched Cr(VI) is mixed with the unfractionated input solution by hydrodynamic advection and dispersion. Advection and dispersion could result in less enriched δ^{53}Cr values than expected for closed systems.

A fractionation factor of 0.9979 was determined using Equation 3.2 and a linear regression through all of the data (effluent and profiles). This indicates less extensive fractionation than previously reported by Ellis et al. (2002), where the α value for Cr(VI) reduction by magnetite was found to be 0.9965. Investigations into Cr(VI) sorption by goethite and aluminum oxide determined that the effect of sorption on Cr isotope fractionation was negligible (Ellis et al., 2004). More recently, Døssing et al. (2011) obtained a fractionation factor of 0.9985 for Cr(VI) reduction by aqueous Fe(II), which they concluded to be the result of a combination of two reduction mechanisms: direct reduction by $Fe(II)_{aq}$ that produced an isotopic fractionation, and sorption and subsequent reduction by green rust that did not result in a measurable fractionation. The α value of 0.9979 obtained in this study also suggests Cr(VI) reduction due to a combination of mechanisms, and is similar to the value determined by Døssing et al. (2011). Calculations using α values of 0.9965 for reduction in solution and 1.0000 for sorption (Ellis et al., 2002, 2004) indicate that ~60% of the Cr(VI) was reduced in solution, while ~40% underwent sorption prior to reduction to Cr(III). Both the results of the

solid-phase Cr and isotope analyses suggest a combination of Cr(VI) reduction mechanisms, such as those proposed by Park et al. (2005).

The "reservoir effect" described by Berna et al. (2010) also may diminish the apparent Cr isotope fractionation observed under saturated flow conditions. Organic carbon comprised only 10% (v/v) of the column matrix. If reduction had occurred in association with the organic carbon, and no reduction is caused by the quartz sand, it is reasonable to assume that heterogeneous reduction occurred. The mixing of pore water in contact with the organic carbon with water from the sand areas of the column likely produced an average δ^{53}Cr smaller than the intrinsic fractionation due to organic carbon alone (Berna et al., 2010).

3.4.4 Implications for Tracking Cr(VI) Migration in Groundwater

Chromium isotopes can be used as a tool for tracking reduction in natural systems if there is a full understanding of the nature of the fractionation. Ellis et al. (2002) have provided a baseline fractionation factor for abiotic reduction in solution. However, additional mechanisms of Cr(VI) removal are possible (Palmer and Wittbrodt, 1991). Although preliminary attempts to utilize Cr isotopes to track Cr(VI) migration have been made (Ellis et al., 2004; Izbicki et al., 2008; Berna et al., 2010; Raddatz et al., 2011), assuming that a single fractionation factor applies to mechanisms of Cr(VI) removal in all settings may not be suitable. The influence of transport on Cr isotope fractionation also presents another potential complication to the application of Cr isotopes to field studies. Previous attempts to fit field data to a fractionation curve have assumed a Rayleigh model (Izbicki et al., 2008; Raddatz et al., 2011); however, the

results of this study suggested that the shape of the isotope fractionation curve may be influenced by transport in the plume.

Chromium isotopes remain a potential tool for tracking Cr(VI) migration in groundwater. Characterization of local fractionation factors will provide further insight into the conditions and mechanisms present in different contaminated areas. Recent studies demonstrate that Cr isotope fractionation during reduction may be more complex than initially anticipated (Berna et al., 2010; Døssing et al., 2011). By combining multiple approaches, including standard geochemical analyses, Cr isotope measurements, and spectroscopic techniques such as SEM and XANES, our ability to describe these complex systems can be improved.

3.5 Conclusions

- Removal of Cr(VI) by organic carbon under saturated flow conditions was accompanied by an enrichment in $\delta^{53}Cr$ which followed a linear trend described by $\alpha = 0.9979$.
- Isotope results indicated a combination of two Cr(VI) removal mechanisms: (I) direct reduction in solution localized around the organic carbon particles, and (II) sorption of Cr(VI) to the organic carbon followed by reduction.
- Observations of solid-phase Cr(III) on the organic carbon indicated that reduction of Cr(VI) had occurred.
- The application of multiple analytical techniques was essential for interpreting the results of this column study.

- The linear trend of the isotope data may indicate an influence of transport on Cr isotope fractionation under saturated flow conditions. Further investigation of this possible influence is necessary prior to the application of Cr isotopes for tracking the migration of Cr(VI)-contaminated groundwater in a field setting.

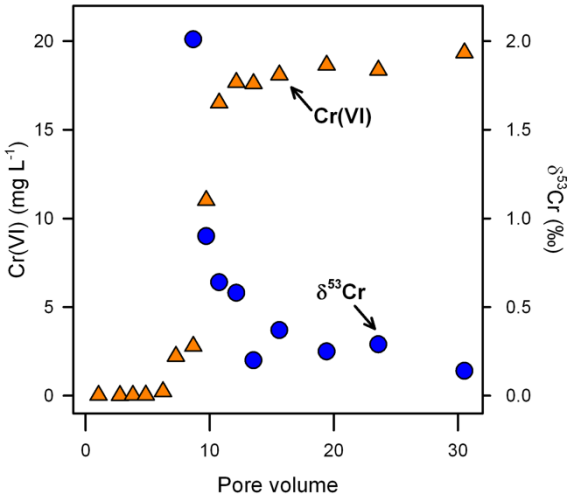

Figure 3.1 Effluent Cr(VI) concentration and corresponding δ^{53}Cr values over 30 pore volumes (88 days). Breakthrough occurred after approximately 12 pore volumes.

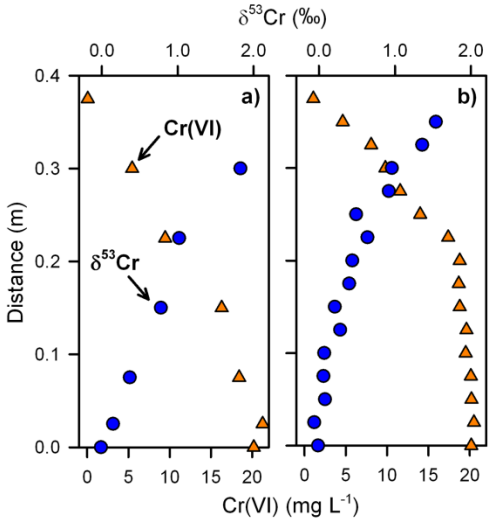

Figure 3.2 Profile Cr(VI) concentration and corresponding $\delta^{53}Cr$ values taken after approximately a) 5.5 PVs and b) 8.5 PVs.

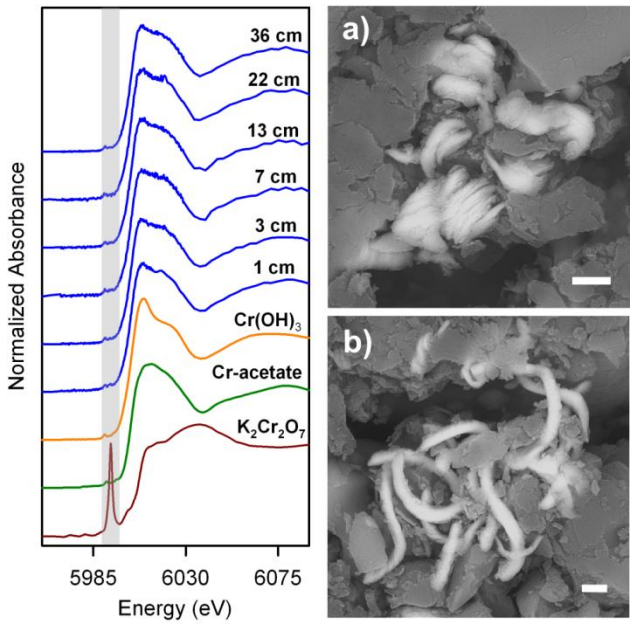

Figure 3.3 XANES spectra collected for $Cr(OH)_3$, Cr-acetate, and $K_2Cr_2O_7$ standards and for Cr on the organic carbon particles at each position sampled along the column starting from the input at 1 cm. The spectra for the column samples indicate the Cr spectra most closely resemble spectra for $Cr(OH)_3$ and Cr-acetate standards, suggesting the Cr is present primarily as Cr(III). The shaded region indicates the position of the characteristic Cr(VI) pre-edge feature, with negligible Cr(VI) in the column samples. SEM images show chromium-bearing precipitates observed on organic carbon particles collected 1 cm from the column input (a & b). Scale bar represents 2 μm.

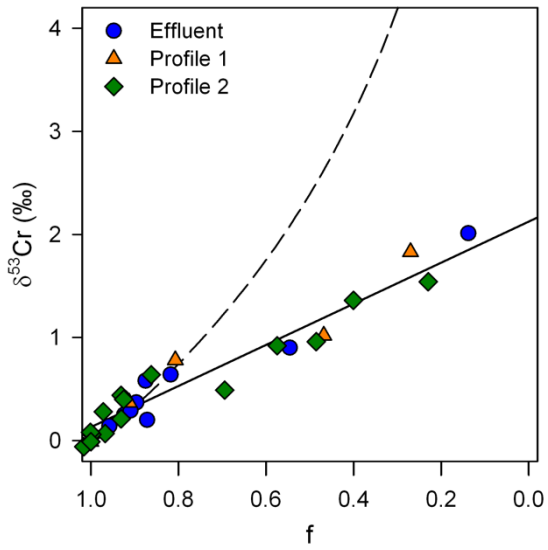

Figure 3.4 Isotope results for the effluent samples and both profiles. A linear regression on the pooled data results in $\alpha = 0.9979$ (solid line). The dashed line represents a Rayleigh curve with $\alpha = 0.9965$.

Chapter 4:

Conclusions

4.1 Summary of Findings

Changes in $\delta^{53}Cr$ are indicative of mass-transfer processes. As such, measurements of Cr isotopes have been proposed as a means of tracking Cr(VI) migration in groundwater (Blowes, 2002; Ellis et al., 2002). Previously published results have demonstrated that the extent of $\delta^{53}Cr$ enrichment depends on the reactive material and the mechanism of Cr(VI) removal (Ellis et al., 2002, 2004; Sikora et al., 2008; Berna et al., 2010; Zink et al., 2010; Døssing et al., 2011). Results from this thesis contribute to a more complete understanding of the factors that control Cr isotope fractionation under various conditions.

Laboratory batch experiments using granular zero-valent iron (ZVI) and organic carbon (OC) were conducted to characterize the extent of Cr isotope fractionation during reduction of Cr(VI) (Chapter 2). Decreases in Cr(VI) concentrations were accompanied by increases in $\delta^{53}Cr$ values for all ZVI experiments. Rayleigh-type fractionation was observed in the ZVI experiments, suggesting that the reduced Cr(III) was effectively isolated from the remaining Cr(VI) pool. Despite a wide range of reaction rates, fractionation factors (α) were very similar for all ZVI experiments, varying only from 0.9993 to 0.9995. Assuming $\alpha = 1.0000$ for sorption of Cr(VI) (Ellis et al., 2004) and $\alpha = 0.9965$ for homogeneous reduction of Cr(VI) in solution (Ellis et al., 2002), the isotope results in Chapter 2 suggest that Cr(VI) removal by ZVI occurred primarily as a result of sorption. Solid-phase Cr analysis by XANES, SEM, and XPS

indicated that only reduced Cr(III) was present on the surface of the reactive material, suggesting that the Cr(VI) was rapidly reduced following sorption, and that any Cr(VI) reduced in solution was immediately precipitated. Characterization of the mechanism of Cr(VI) removal by ZVI and the associated isotope fractionation is crucial for the application of Cr isotopes for tracking Cr(VI) migration in groundwater undergoing remediation by ZVI.

Several potential influences on Cr isotope fractionation were considered, including pre-treatment of the ZVI, experimental design, and changes in reaction rate. Although removing the oxidized coating from the ZVI during pre-treatment resulted in an increased Cr(VI) removal rate, the isotope results were very similar, suggesting that the mechanism of removal was also similar. A comparison of single- vs. multi-flask experimental design resulted in almost no difference in the isotope fractionation. Nonetheless, a multi-flask design is preferable so that solid-phase analyses can be performed vs. time. Finally, changes in reaction rate induced by adjusting the mass of reactive material also resulted in no difference in isotope fractionation.

The interpretation of the isotope results for the organic carbon batch experiments was complicated by a large discrepancy between Cr(VI) and Cr_{TOT} measurements, suggesting that Cr(III) was not completely removed from solution. The sample preparation method for Cr isotope analysis was not designed to process samples with a mixture of Cr(VI) and Cr(III) in solution. As a result, the isotope data for these experiments were influenced by a positive $\delta^{53}Cr$ contribution from the Cr(VI) and a negative $\delta^{53}Cr$ contribution from the Cr(III). Further development of the sample preparation method is required to discern the true Cr isotope fractionation trend for these samples.

Results from the column study presented in Chapter 3 also exhibited decreasing Cr(VI) concentrations accompanied by increasing δ^{53}Cr values. Unlike the batch experiments in Chapter 2, the isotope data did not follow a Rayleigh-type fractionation; instead, a linear trend was fitted with a fractionation factor $\alpha = 0.9979$. Park et al. (2005) proposed that two possible mechanisms of Cr(VI) removal by organic carbon exist: (I) direct reduction in solution, and (II) sorption of Cr(VI) followed by reduction. The isotope results in Chapter 3 suggest that Cr(VI) removal in the column occurred through a mixture of the two mechanisms, where Mechanism I would produce an isotope fractionation with $\alpha = 0.9965$ and Mechanism II would cause no measurable fractionation ($\alpha = 1.0000$). Analyses of solid-phase Cr by SEM and XANES indicated the presence of only Cr(III) as $Cr(OH)_3$ or Cr-acetate, consistent with the reaction mechanism inferred from the Cr isotopes.

Chapter 3 reported the first results that demonstrate Cr isotope fractionation during reduction under transport conditions. Numerous batch experiments presented in the literature (Ellis et al., 2002; Sikora et al., 2008; Berna et al., 2010) strongly suggest that Cr fractionation follows a Rayleigh model, so it is reasonable to speculate that the linear behaviour of the isotope data can be attributed to transport effects. This observation suggests that an analogous batch experiment in the absence of transport would exhibit Rayleigh-type fractionation similar to the vast majority of the experiments in the literature.

4.2 Recommendations

Chromium isotopes are a promising tool for tracking Cr(VI) migration in groundwater. However, results from this thesis reinforce the need to characterize the degree of fractionation prior to the application of this tool to a field setting. Reduction of Cr(VI) can be accomplished using a variety of electron donors, including magnetite, Fe(II), ZVI, organic carbon, H_2O_2, and bacteria. Both published results and data from this thesis demonstrate that Cr isotope fractionation varies significantly depending on the reductant. Further laboratory experiments should be conducted to evaluate the fractionation associated with materials intended for use in Cr(VI) treatment. Batch experiments should be performed on reactive material sampled from Cr(VI)-contaminated field sites, whether it is the natural substrate or an engineered PRB, to identify the removal mechanism and associated isotope fractionation. Results in this thesis have shown that multiple analytical approaches, such as traditional geochemical measurements, Cr isotopes, and solid-phase analyses, are essential for building a complete understanding of the Cr(VI) treatment mechanism. In addition, laboratory column experiments using a variety of reactive materials will be necessary to further investigate the possible influence of transport on Cr isotope fractionation under saturated flow conditions. These laboratory-scale studies will provide insight into the behaviour of Cr isotope fractionation during Cr(VI) reduction under a variety of conditions, and will thus facilitate the interpretation of field data.

The method of sample preparation for Cr isotope analysis described in this thesis was designed with the expectation that all Cr in solution is in the form of Cr(VI). Samples from the organic carbon batch experiments appeared to contain a mixture of Cr(VI) and Cr(III), even

after filtering. As a result, it was not possible to acquire reliable results for the isotope composition of the Cr(VI) in these samples. It would be beneficial to adapt the sample preparation method so that samples such as these can be analyzed for Cr isotopes. Further batch experiments using organic carbon should be conducted to investigate the mechanism of Cr(VI) removal and determine the form of Cr(III), as well as to characterize the Cr isotope fractionation.

References

Amos, R.T., Mayer, K.U., Blowes, D.W., Ptacek, C.J., 2004. Reactive transport modeling of column experiments for the remediation of acid mine drainage. *Environ. Sci. Technol.* 38(11), 3131-3138.

Ball, J.W., Bassett, R.L., 2000. Ion exchange separation of chromium from natural water matrix for stable isotope mass spectrometric analysis. *Chem. Geol.* 168(1-2), 123-134.

Benner, S.G., Blowes, D.W., Ptacek, C.J., 1997. A full-scale porous reactive wall for prevention of acid mine drainage. *Ground Water Monit. Rem.* 17(4), 99-107.

Berna, E.C., Johnson, T.M., Makdisi, R.S., Basu, A., 2010. Cr stable isotopes as indicators of Cr(VI) reduction in groundwater: A detailed time-series study of a point-source plume. *Environ. Sci. Technol.* 44(3), 1043-1048.

Blowes, D.W., 2002. Tracking hexavalent Cr in groundwater. *Science* 295(5562), 2024-2025.

Blowes, D.W., Ptacek, C.J., Benner, S.G., McRae, C.W.T., Bennett, T.A., Puls, R.W., 2000. Treatment of inorganic contaminants using permeable reactive barriers. *J. Contam. Hydrol.* 45(1-2), 123-137.

Blowes, D.W., Ptacek, C.J., Jambor, J.L., 1997. In-situ remediation of Cr(VI)-contaminated groundwater using permeable reactive walls: Laboratory studies. *Environ. Sci. Technol.* 31(12), 3348-3357.

Bolan, N.S., Adriano, D.C., Natesan, R., Koo, B.-J., 2003. Effects of organic amendments on the reduction and phytoavailability of chromate in mineral soil. *J. Environ. Qual.* 32(1), 120-128.

Brunauer, S., Emmett, P.H., Teller, E., 1938. Adsorption of gases in multimolecular layers. *J. Am. Chem. Soc.* 60(2), 309-319.

Clark, I., Fritz, P. (1997). Environmental Isotopes in Hydrogeology. New York, NY, CRC Press.

Cummings, D.E., Fendorf, S., Singh, N., Sani, R.K., Peyton, B.M., Magnuson, T.S., 2006. Reduction of Cr(VI) under acidic conditions by the facultative Fe(III)-reducing bacterium *Acidiphilium cryptum*. *Environ. Sci. Technol.* 41(1), 146-152.

Døssing, L.N., Dideriksen, K., Stipp, S.L.S., Frei, R., 2011. Reduction of hexavalent chromium by ferrous iron: A process of chromium isotope fractionation and its relevance to natural environments. *Chem. Geol.* 285(1-4), 157-166.

Dutta, R., Mohammad, S.S., Chakrabarti, S., Chaudhuri, B., Bhattacharjee, S., Dutta, B.K., 2010. Reduction of hexavalent chromium in aqueous medium with zerovalent Iron. *Water Environ. Res.* 82(2), 138-146.

Eary, L.E., Rai, D., 1988. Chromate removal from aqueous wastes by reduction with ferrous ion. *Environ. Sci. Technol.* 22(8), 972-977.

Ellis, A.S., Johnson, T.M., Bullen, T.D., 2002. Chromium isotopes and the fate of hexavalent chromium in the environment. *Science* 295(5562), 2060-2062.

Ellis, A.S., Johnson, T.M., Bullen, T.D., 2004. Using chromium stable isotope ratios to quantify Cr(VI) reduction: Lack of sorption effects. *Environ. Sci. Technol.* 38(13), 3604-3607.

Frei, R., Rosing, M.T., 2005. Search for traces of the late heavy bombardment on Earth--Results from high precision chromium isotopes. *Earth Planet. Sci. Lett.* 236(1-2), 28-40.

Gheju, M., 2011. Hexavalent chromium reduction with zero-valent iron (ZVI) in aquatic systems. *Water Air Soil Pollut.* 222(1-4), 103-148.

Gould, J.P., 1982. The kinetics of hexavalent chromium reduction by metallic iron. *Water Res.* 16(6), 871-877.

Greenberg, A.E., Cleceri, L.S., Eaton, A.D., Eds. (1992). Standard Methods for the Examination of Water and Wastewater. Washington, DC, American Health Association.

Gui, L., Yang, Y., Jeen, S.-W., Gillham, R.W., Blowes, D.W., 2009. Reduction of chromate by granular iron in the presence of dissolved CaCO3. *Appl. Geochem.* 24(4), 677-686.

Izbicki, J.A., Ball, J.W., Bullen, T.D., Sutley, S.J., 2008. Chromium, chromium isotopes and selected trace elements, western Mojave Desert, USA. *Appl. Geochem.* 23(5), 1325-1352.

Jeen, S.-W. (2005). Effects of Mineral Precipitation on Long-Term Performance of Granular Iron Permeable Reactive Barriers. Ph.D., University of Waterloo.

Jeen, S.-W., Blowes, D.W., Gillham, R.W., 2008. Performance evaluation of granular iron for removing hexavalent chromium under different geochemical conditions. *J. Contam. Hydrol.* 95(1-2), 76-91.

Jeen, S.W., Jambor, J.L., Blowes, D.W., Gillham, R.W., 2007. Precipitates on granular iron in solutions containing calcium carbonate with trichloroethene and hexavalent chromium. *Environ. Sci. Technol.* 41(6), 1989-1994.

Light, T.S., 1972. Standard solution for redox potential measurements. *Anal. Chem.* 44(6), 1038-1039.

Lindsay, M.B.J., Ptacek, C.J., Blowes, D.W., Gould, W.D., 2008. Zero-valent iron and organic carbon mixtures for remediation of acid mine drainage: Batch experiments. *Appl. Geochem.* 23(8), 2214-2225.

Losi, M.E., Amrhein, C., Frankenberger Jr, W.T., 1994. Environmental biochemistry of chromium. *Rev. Environ. Contam. Toxicol.* 136, 91-121.

Lovley, D.R., Phillips, E.J.P., 1994. Reduction of chromate by *Desulfovibrio vulgaris* and its *c3* cytochrome. *Appl. Environ. Microbiol.* 60(2), 726-728.

Mayer, K.U. (1999). A Numerical Model for Multicomponent Reactive Transport in Variably Saturated Porous Media. Ph.D., University of Waterloo.

Mayer, K.U., Blowes, D.W., Frind, E.O., 2001. Reactive transport modeling of an in situ reactive barrier for the treatment of hexavalent chromium and trichloroethylene in groundwater. *Water Resour. Res.* 37(12), 3091-3103.

Nordstrom, D.K., 1977. Thermochemical redox equilibria of ZoBell's solution. *Geochim. Cosmochim. Acta* 41(12), 1835-1841.

Nordstrom, D.K., Wilde, F.D., 2006, Reduction-oxidation potential (electrode method) (ver. 1.2): U.S. Geological Survey Techniques of Water-Resources Investigations, book 9, chap. A6, sec. 6.5, July 2006, accessed December 7, 2011, from http://pubs.water.usgs.gov/twri9A6/.

O'Brien, P., Kortenkamp, A., 1994. Chemical models important in understanding the ways in which chromate can damage DNA. *Environ. Health Perspect.* 102(SUPPL. 3), 3-10.

Palmer, C.D., Wittbrodt, P.R., 1991. Processes affecting the remediation of chromium-contaminated sites. *Environ. Health Perspect.* 92, 25-40.

Park, D., Ahn, C.K., Kim, Y.M., Yun, Y.-S., Park, J.M., 2008. Enhanced abiotic reduction of Cr(VI) in a soil slurry system by natural biomaterial addition. *J. Hazard. Mater.* 160(2-3), 422-427.

Park, D., Lim, S.-R., Yun, Y.-S., Park, J.M., 2007. Reliable evidences that the removal mechanism of hexavalent chromium by natural biomaterials is adsorption-coupled reduction. *Chemosphere* 70(2), 298-305.

Park, D., Yun, Y.-S., Hye Jo, J., Park, J.M., 2005. Mechanism of hexavalent chromium removal by dead fungal biomass of Aspergillus niger. *Water Res.* 39(4), 533-540.

Raddatz, A.L., Johnson, T.M., McLing, T.L., 2011. Cr stable isotopes in Snake River Plain Aquifer groundwater: Evidence for natural reduction of dissolved Cr(VI). *Environ. Sci. Technol.* 45(2), 502-507.

Rai, D., Sass, B.M., Moore, D.A., 1987. Chromium(III) hydrolysis constants and solubility of chromium(III) hydroxide. *Inorg. Chem.* 26(3), 345-349.

Ravel, B., Newville, M., 2005. ATHENA, ARTEMIS, HEPHAESTUS: Data analysis for X-ray absorption spectroscopy using IFEFFIT. *J. Synchrotron Radiat.* 12(4), 537-541.

Schauble, E., Rossman, G.R., Taylor Jr, H.P., 2004. Theoretical estimates of equilibrium chromium-isotope fractionations. *Chem. Geol.* 205(1-2), 99-114.

Schoenberg, R., Zink, S., Staubwasser, M., von Blanckenburg, F., 2008. The stable Cr isotope inventory of solid Earth reservoirs determined by double spike MC-ICP-MS. *Chem. Geol.* 249(3-4), 294-306.

Sevim, F., Demir, D., 2008. Investigation of reduction kinetics of $Cr_2O_7^{2-}$ in $FeSO_4$ solution. *Chem. Eng. J.* 143(1-3), 161-166.

Siebert, C., Nägler, T.F., Kramers, J.D., 2001. Determination of molybdenum isotope fractionation by double-spike multicollector inductively coupled plasma mass spectrometry. *Geochem. Geophys. Geosyst.* 2(7).

Sikora, E.R., Johnson, T.M., Bullen, T.D., 2008. Microbial mass-dependent fractionation of chromium isotopes. *Geochim. Cosmochim. Acta* 72(15), 3631-3641.

Tokunaga, T.K., Wan, J., Firestone, M.K., Hazen, T.C., Olson, K.R., Herman, D.J., Sutton, S.R., Lanzirotti, A., 2003. In situ reduction of chromium(VI) in heavily contaminated soils through organic carbon amendment. *J. Environ. Qual.* 32(5), 1641-1649.

Wittbrodt, P.R., Palmer, C.D., 1995. Reduction of Cr(VI) in the Presence of Excess Soil Fulvic Acid. *Environ. Sci. Technol.* 29(1), 255-263.

Zink, S., Schoenberg, R., Staubwasser, M., 2010. Isotopic fractionation and reaction kinetics between Cr(III) and Cr(VI) in aqueous media. *Geochim. Cosmochim. Acta* 74(20), 5729-5745.

Appendix A:

Summary of Data Presented in Chapter 2

Table A.1 Summary of general chemistry and Cr concentrations for multi-flask batch experiments.

Sample	Time (days)	pH	Eh (mV)	Concentration (mg L^{-1})		
				Alk	Cr(VI)	Cr_{TOT}
ZVI-MA	0.0	4.91	-210	3.5	52	49
	0.2	6.22	225	7.5	40	38
	0.4	6.70	240	8.5	39	37
	0.6	6.92	245	16	30	28
	0.8	6.32	250	11	35	33
	1.0	6.63	240	14	32	30
	1.3	7.45	305	22	25	23
	3.0	9.48	-490	25	20	20
ZVI-MB*	0.0	5.44	585	1.5	46	47
	1.0	6.75	435	21	25	25
	2.0	9.25	380	23	19	19
	3.0	10.11	340	26	15	15
		10.25	325	29	14	14
	4.0	10.58	320	32	9.0	9.6
	4.2	10.59	280	33	8.0	8.0
		10.45	200	35	9.0	8.8
	4.8	10.58	305	29	7.0	7.5
		10.66	245	25	6.0	6.5
	5.3	10.64	285	33	5.1	5.0
		10.65	135	35	5.7	5.3
	6.0	10.67	255	33	5.6	5.4
		10.64	120	34	2.6	2.4
	6.4	10.65	260	34	5.2	4.8
		10.72	220	37	3.5	3.2
	7.0	10.69	225	37	2.8	2.8
	7.4	10.67	250	36	3.7	3.5
	9.2	10.72	195	39	0.80	< 0.12
	10.1	10.71	205	34	0.22	n/d
	11.1	10.71	225	36	0.13	n/d
	CONTROL	9.14	295	3.5	0.00	n/d

Alk = total alkalinity as mg L^{-1} $CaCO_3$; * = replicate experiment presented in main body; n/a = parameter not measured; n/d = below MDL

Table A.1 Continued.

Sample	Time (days)	pH	Eh (mV)	Concentration (mg L^{-1})		
				Alk	Cr(VI)	Cr_{TOT}
ZVI-MP*	0.00	8.77	370	128	42	46
	0.04	9.42	385	110	27	26
	0.07	9.45	125	118	21	23
	0.10	n/a	n/a	n/a	29	27
	0.14	n/a	n/a	n/a	23	25
	0.28	n/a	n/a	n/a	17	18
	0.46	n/a	n/a	n/a	17	17
		9.67	215	78	13	13
	0.94	n/a	n/a	n/a	7.0	7.9
		n/a	n/a	n/a	8.5	8.7
	1.2	9.74	-135	63	5.7	6.8
		n/a	n/a	n/a	6.5	7.3
	1.5	n/a	n/a	n/a	4.1	3.0
		n/a	n/a	n/a	5.7	6.1
	2.0	9.91	-170	56	2.0	1.6
		n/a	n/a	n/a	1.6	1.6
	2.3	n/a	n/a	n/a	1.3	1.0
		n/a	n/a	n/a	1.4	0.98
	3.0	n/a	n/a	n/a	0.64	0.48
		n/a	n/a	n/a	0.76	0.62
	4.2	9.96	115	58	0.07	0.07
OC-MA	0.00	4.94	425	2.0	51	49
	0.09	7.29	-40	75	40	34
	0.93	9.23	-470	92	32	29
	1.8	8.44	-435	94	35	31
	4.8	9.08	-390	140	25	21
	24	9.13	-395	206	0.20	8.3
OC-MB*	0.00	5.39	615	1.5	50	46
	1.0	8.56	390	110	22	17
	2.0	9.25	330	110	3.1	9.8
	2.3	9.29	260	120	0.90	4.9
	3.0	9.28	310	135	0.04	3.7
	CONTROL	8.87	-65	141	0.05	0.01

Alk = total alkalinity as mg L^{-1} $CaCO_3$; * = replicate experiment presented in main body; n/a = parameter not measured; n/d = below MDL

Table A.2 Summary of Cr concentrations for single-flask batch experiments.

Sample	**Time (h)**	**Cr(VI) ($mg\ L^{-1}$)**	**Cr_{TOT} ($mg\ L^{-1}$)**
ZVI-S10A*	0.0	52	52
	0.3	48	50
	0.5	48	47
	1.0	44	43
	6.6	31	30
	19.2	11	11
	25.5	3.1	3.1
	67.5	0.10	0.05
	CONTROL	n/a	0.01
ZVI-S10B	0.0	51	44
	0.5	46	43
	2.0	39	35
	6.3	25	27
	10.7	20	19
	19.9	9.2	10
	27.7	4.7	5.1
	50.9	0.28	0.30
ZVI-S100A*	0.0	52	49
	0.3	39	36
	0.7	21	20
	1.0	7.0	7.1
	1.2	1.4	0.94
	1.3	0.00	0.02
	1.4	0.00	0.001
	CONTROL	n/a	0.001
ZVI-S100B	0.0	51	44
	0.3	32	28
	0.4	20	17
	0.6	12	11
	0.7	10	9.3
	0.9	0.02	0.001
	1.0	0.00	0.001

* = replicate experiment presented in main body

Table A.3 Summary of Cr isotope data for batch experiments.

Sample	Time (days)	f	δ^{53}Cr (‰)	±1σ (‰)
ZVI-MA	0.0	1.00	-0.08	0.08
	0.2	0.78	0.04	0.08
	0.4	0.75	0.08	0.08
	0.6	0.56	0.20	0.07
	0.8	0.67	0.10	0.07
	1.0	0.61	0.20	0.09
	1.3	0.47	0.31	0.07
	3.0	0.40	0.41	0.08
ZVI-MB*	0.0	1.00	0.00	0.08
	1.0	0.53	0.35	0.11
	2.0	0.39	0.46	0.08
	3.0	0.31	0.62	0.10
		0.29	0.60	0.07
	4.0	0.20	1.03	0.08
	4.2	0.17	1.16	0.10
		0.19	0.92	0.09
	4.8	0.16	1.05	0.07
		0.14	1.12	0.07
	5.3	0.11	1.31	0.07
		0.11	1.23	0.07
	6.0	0.12	1.20	0.07
		0.05	1.64	0.07
	6.4	0.10	1.36	0.09
		0.07	1.69	0.07
	7.0	0.06	1.85	0.10
	7.4	0.07	1.59	0.10
	9.2	0.00012	n/a	n/a
	10.1	0.00005	n/a	n/a
	11.1	0.00010	n/a	n/a

* = replicate experiment presented in main body; n/a = parameter not measured (Cr concentration too low for isotope analysis)

Table A.3 Continued.

Sample	Time (days)	f	$\delta^{53}Cr$ (‰)	±1σ (‰)
ZVI-MP*	0.00	1.00	0.07	0.10
	0.04	0.57	0.50	0.09
	0.07	0.51	0.54	0.09
	0.10	0.58	0.51	0.10
	0.14	0.54	0.50	0.09
	0.28	0.39	0.72	0.09
	0.46	0.37	0.70	0.10
		0.27	0.93	0.10
	0.94	0.17	1.04	0.09
		0.19	1.08	0.10
	1.2	0.15	1.16	0.11
		0.16	1.14	0.09
	1.5	0.09	1.37	0.09
		0.13	1.24	0.09
	2.0	0.05	n/a	n/a
		0.05	n/a	n/a
	2.3	0.03	n/a	n/a
		0.03	n/a	n/a
	3.0	0.01	n/a	n/a
		0.02	n/a	n/a
	4.2	0.002	n/a	n/a
OC-MA	0.00	1.00	-0.05	0.09
	0.09	0.70	0.14	0.09
	0.93	0.59	0.45	0.09
	1.8	0.62	0.27	0.09
	4.8	0.43	0.53	0.08
	24	0.17	-0.45	0.10
OC-MB*	0.00	1.00	0.01	0.09
	1.0	0.36	0.61	0.08
	2.0	0.21	0.86	0.09
	2.3	0.11	1.03	0.09
	3.0	0.08	n/a	n/a

* = replicate experiment presented in main body; n/a = parameter not measured (Cr concentration too low for isotope analysis)

Table A.3 Continued.

Sample	Time (h)	f	$\delta^{53}Cr$ (‰)	±1σ (‰)
ZVI-S10A*	0.0	1.00	-0.03	0.09
	0.3	0.97	-0.01	0.10
	0.5	0.92	-0.06	0.08
	1.0	0.83	-0.03	0.09
	6.6	0.59	0.16	0.09
	19.2	0.21	0.93	0.11
	25.5	0.06	1.98	0.13
	67.5	0.001	n/a	n/a
ZVI-S10B	0.0	1.00	0.06	0.08
	0.5	0.96	0.01	0.10
	2.0	0.80	0.05	0.07
	6.3	0.62	0.16	0.08
	10.7	0.43	0.30	0.08
	19.9	0.22	0.61	0.08
	27.7	0.12	0.95	0.09
	50.9	0.01	n/a	n/a
ZVI-S100A*	0.0	1.00	-0.03	0.09
	0.3	0.74	0.13	0.08
	0.7	0.41	0.36	0.08
	1.0	0.15	1.10	0.12
	1.2	0.02	2.26	0.13
	1.3	0.0005	n/a	n/a
	1.4	0.00002	n/a	n/a
ZVI-S100B	0.0	1.00	0.06	0.08
	0.3	0.63	0.24	0.10
	0.4	0.39	0.44	0.09
	0.6	0.26	0.64	0.08
	0.7	0.21	0.69	0.09
	0.9	0.00003	n/a	n/a
	1.0	0.00001	n/a	n/a

* = replicate experiment presented in main body; n/a = parameter not measured (Cr concentration too low for isotope analysis)

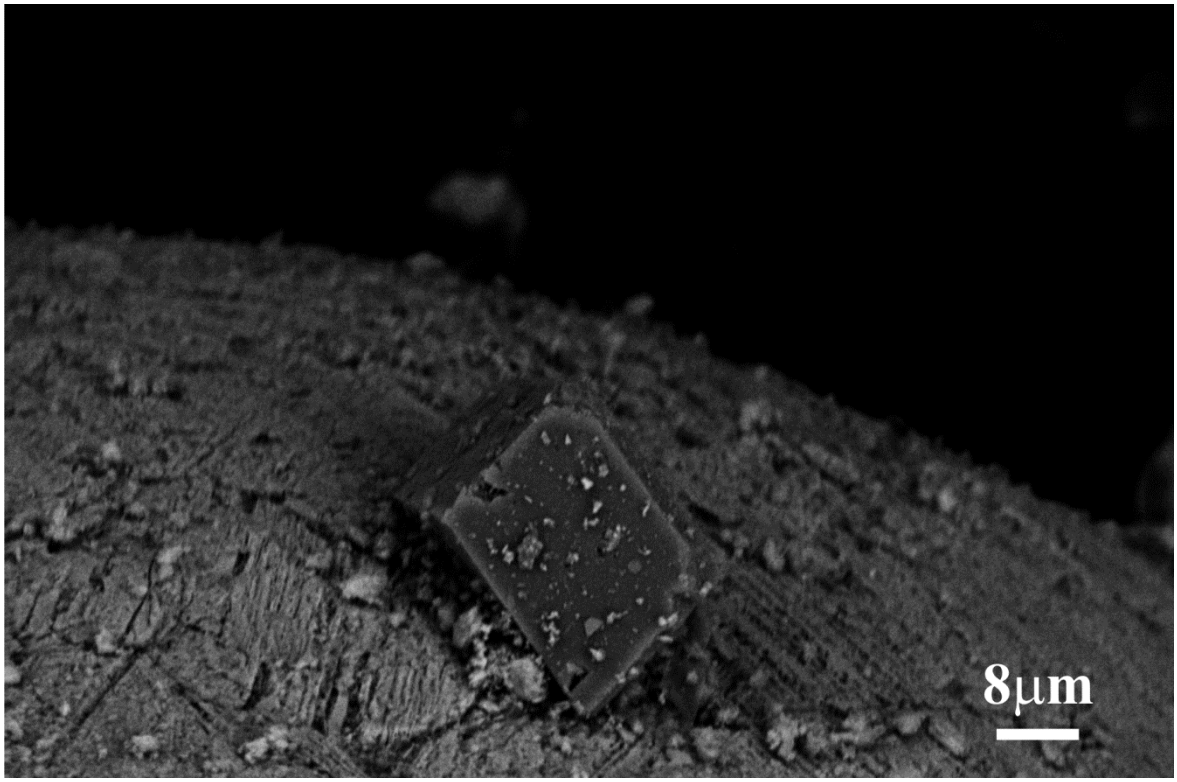

Figure A.1 Backscatter SEM image of a rhombohedral calcite crystal observed on the solid material from the ZVI-MP batch experiment.

Appendix B:

Summary of Data Presented in Chapter 3

Table B.1 Summary of general chemistry and cation concentrations for input and effluent column samples.

Sample	PVs	pH	Eh	Concentration (mg L^{-1})				
			(mV)	Alk	Cr(VI)	Cr	Ca	K
input	2.8	5.40	655	77	20	21	34	21
	4.9	5.61	605	88	20	21	32	17
	5.9	5.74	605	87	20	21	32	17
	10.8	7.78	490	58	20	21	33	17
	11.1	6.92	470	50	20	20	37	16
	14.9	7.50	n/a	79	20	20	37	17
	23.9	8.01	540	75	20	20	38	16
effluent	2.8	8.04	455	766	0.00	0.17	312	12
	3.8	6.92	535	511	0.00	0.10	241	20
	4.9	6.70	520	508	0.00	0.08	183	21
	6.2	6.74	515	469	0.11	0.21	239	25
	7.3	6.87	525	341	0.29	1.9	119	17
	8.7	7.23	465	291	1.9	2.8	113	17
	9.7	7.23	465	154	11	11	55	14
	10.8	7.48	430	137	17	17	46	16
	12.1	7.37	460	96	18	18	43	21
	13.5	7.09	415	93	18	18	44	17
	15.6	7.08	525	112	18	18	43	17
	19.4	6.87	495	104	18	19	40	17
	23.6	7.41	440	96	19	18	54	23
	30.5	7.20	595	75	20	19	42	17

Alk = total alkalinity as mg L^{-1} $CaCO_3$; n/a = parameter not measured

Table B.2 Summary of general chemistry and cation concentrations for column profile samples. Profile 1 was sampled at 5.5 PVs, Profile 2 was sampled at 8.5 PVs.

Sample	Distance (m)	pH	Eh (mV)	Concentration (mg L^{-1})				
				Alk	Cr(VI)	Cr	Ca	K
Profile 1	0.025	6.01	568	80	20	21	45	18
	0.075	6.35	533	195	19	18	74	20
	0.150	6.48	540	340	16	16	122	17
	0.225	6.62	533	395	8.6	9.5	136	18
	0.300	6.90	519	450	4.8	5.5	154	22
	0.375	6.67	456	445	0.00	0.06	195	19
Profile 2	0.025	n/a	n/a	n/a	21	21	32	17
	0.050	n/a	n/a	n/a	21	20	34	20
	0.075	n/a	n/a	n/a	20	20	37	17
	0.100	n/a	n/a	n/a	19	20	44	16
	0.125	n/a	n/a	n/a	19	20	53	14
	0.150	n/a	n/a	n/a	19	19	63	16
	0.175	n/a	n/a	n/a	19	19	70	13
	0.200	n/a	n/a	n/a	18	19	80	14
	0.225	n/a	n/a	n/a	18	17	89	20
	0.250	n/a	n/a	n/a	15	14	83	17
	0.275	n/a	n/a	n/a	12	12	96	20
	0.300	n/a	n/a	n/a	9.7	9.8	97	17
	0.325	n/a	n/a	n/a	8.0	8.1	101	17
	0.350	n/a	n/a	n/a	4.5	4.6	105	17
	0.375	n/a	n/a	n/a	0.92	1.1	110	17

Alk = total alkalinity as mg L^{-1} $CaCO_3$; n/a = parameter not measured

Table B.3 Summary of Cr isotope data for input and effluent column samples.

Sample	PVs	f	δ^{53}Cr (‰)	±1σ (‰)
input	2.8	1.0	0.04	0.10
	4.9	1.0	0.02	0.09
	5.9	1.0	-0.04	0.09
	10.8	1.0	-0.02	0.14
	11.1	1.0	-0.01	0.12
	14.9	1.0	0.00	0.14
	23.9	1.0	-0.04	0.13
effluent	2.8	0.008	n/a	n/a
	3.8	0.005	n/a	n/a
	4.9	0.004	n/a	n/a
	6.2	0.01	n/a	n/a
	7.3	0.09	n/a	n/a
	8.7	0.14	2.01	0.10
	9.7	0.55	0.90	0.14
	10.8	0.82	0.64	0.14
	12.1	0.88	0.58	0.14
	13.5	0.87	0.20	0.13
	15.6	0.90	0.37	0.16
	19.4	0.92	0.25	0.13
	23.6	0.91	0.29	0.11
	30.5	0.96	0.14	0.11

n/a = parameter not measured (Cr concentration too low for isotope analysis)

Table B.4 Summary of Cr isotope data for column profile samples. Profile 1 was sampled at 5.5 PVs, Profile 2 was sampled at 8.5 PVs.

Sample	Distance (m)	f	δ^{53}Cr (‰)	±1σ (‰)
Profile 1	0.025	1.05	0.15	0.11
	0.075	0.91	0.37	0.14
	0.150	0.81	0.78	0.11
	0.225	0.47	1.02	0.12
	0.300	0.27	1.83	0.11
	0.375	0.003	n/a	n/a
Profile 2	0.025	1.02	1.54	0.08
	0.050	1.00	1.36	0.09
	0.075	1.00	0.96	0.08
	0.100	0.97	0.92	0.09
	0.125	0.97	0.49	0.07
	0.150	0.93	0.64	0.08
	0.175	0.93	0.44	0.14
	0.200	0.93	0.40	0.10
	0.225	0.86	0.21	0.09
	0.250	0.69	0.28	0.15
	0.275	0.57	0.07	0.12
	0.300	0.49	0.06	0.07
	0.325	0.40	0.08	0.14
	0.350	0.23	-0.06	0.10
	0.375	0.05	n/a	n/a

n/a = parameter not measured (Cr concentration too low for isotope analysis)

Appendix C:

Double-Spike Inversion Calculation

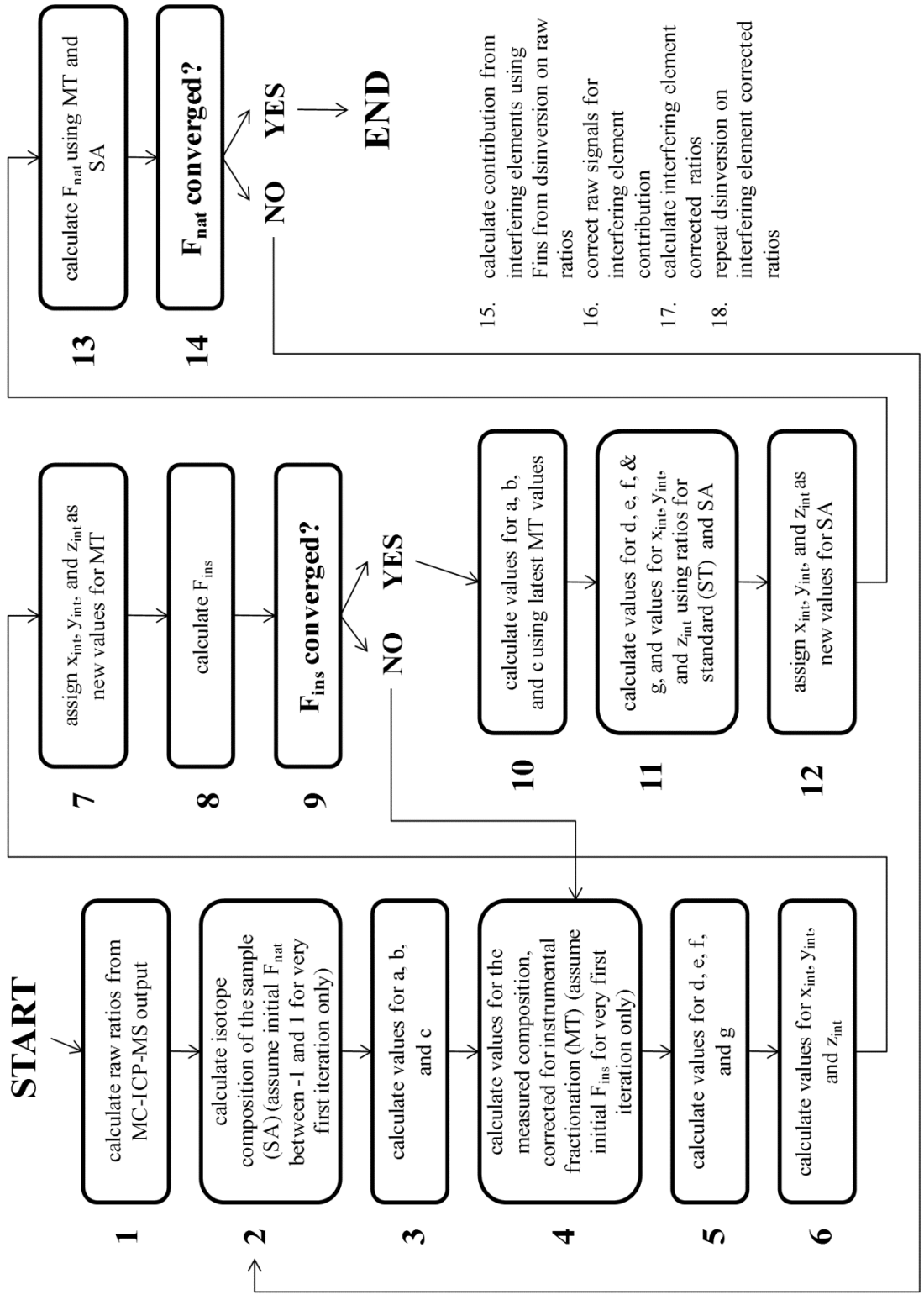

Figure C.1 Flow chart describing the calculation of the true Cr isotope composition of a sample using the double-spike inversion routine adapted from Siebert et al. (2001).

Double-Spike Inversion: Step-by-step

The calculation of the true Cr isotope composition of a sample using the double-spike inversion routine adapted from Siebert et al. (2001).

1. Calculate raw ratios ($^{53}Cr/^{52}Cr$, $^{50}/^{52}Cr$, $^{54}/^{52}Cr$) from uncorrected signals

2. Calculate first assumed isotope composition of sample (SA):

$$R_{sample} = R_{standard}\left(\frac{m_1}{m_2}\right)^{F_{nat}}$$

   - standard (ST) is SRM979
   - assume initial F_{nat} (natural fractionation) between -1 and 1

3. Calculate initial values for a, b, and c:

$$a = \frac{50/52_{ST}(54/52_{SA} - 54/52_{SP}) + 50/52_{SA}(54/52_{SP} - 54/52_{ST}) + 50/52_{SP}(54/52_{ST} - 54/52_{SA})}{50/52_{ST}(53/52_{SA} - 53/52_{SP}) + 50/52_{SA}(53/52_{SP} - 53/52_{ST}) + 50/52_{SP}(53/52_{ST} - 53/52_{SA})}$$

$$b = \frac{53/52_{ST}(54/52_{SA} - 54/52_{SP}) + 53/52_{SA}(54/52_{SP} - 54/52_{ST}) + 53/52_{SP}(54/52_{ST} - 54/52_{SA})}{53/52_{ST}(50/52_{SA} - 50/52_{SP}) + 53/52_{SA}(50/52_{SP} - 50/52_{ST}) + 53/52_{SP}(50/52_{ST} - 50/52_{SA})}$$

$$c = 54/52_{ST} - a53/52_{ST} - b50/52_{ST}$$

   - if F_{nat} is correct, all ratios should lie on the plane z = ax + by + c
   - SP is the double spike composition

4. Calculate initial values for MT:

   - measured, corrected for instrumental fractionation = R_{true}

$$R_{measured} = R_{true}\left(\frac{m_1}{m_2}\right)^{F_{ins}}$$

   - $R_{measured}$ is the raw measured ratio of the spiked sample (MS)
   - assume initial value for F_{ins}

5. Calculate initial values for d, e, f, and g:

$$d = \frac{54/52_{MS} - 54/52_{MT}}{53/52_{MS} - 53/52_{MT}}$$

$$e = 54/52_{MS} - d53/52_{MS}$$

$$f = \frac{54/52_{MS} - 54/52_{MT}}{50/52_{MS} - 50/52_{MT}}$$

$$g = 54/52_{MS} - f50/52_{MS}$$

   - if F_{nat} & F_{ins} are both correct, the line defined by z = dx + e and z = fy + g should intercept with the plane defined by z = ax + by + c

6. Calculate the intersection coordinates of the line with the plane:

$$x_{int} = \frac{bg - be + ef - cf}{af + bd - df}$$

$$y_{int} = \frac{ae - ag + dg - cd}{af + bd - df}$$

$$z_{int} = ax_{int} + by_{int} + c$$

7. Assign x_{int}, y_{int}, and z_{int} as the new values for MT.

   - x_{int} = 53/52, y_{int} = 50/52, z_{int} = 54/52

8. Calculate a new value for F_{ins}:

$$F_{ins} = \frac{\ln (R_{MS}/R_{MT})}{\ln (m_1/m_2)}$$

9. Repeat steps 4-8 iteratively until the value of F_{ins} converges.

10. Calculate values for a, b, and c using the newest values for MT:

$$a = \frac{50/52_{MT}(54/52_{MS} - 54/52_{SP}) + 50/52_{MS}(54/52_{SP} - 54/52_{MT}) + 50/52_{SP}(54/52_{MT} - 54/52_{MS})}{50/52_{MT}(53/52_{MS} - 53/52_{SP}) + 50/52_{MS}(53/52_{SP} - 53/52_{MT}) + 50/52_{SP}(53/52_{MT} - 53/52_{MS})}$$

$$b = \frac{53/52_{MT}(54/52_{MS} - 54/52_{SP}) + 53/52_{MS}(54/52_{SP} - 54/52_{MT}) + 53/52_{SP}(54/52_{MT} - 54/52_{MS})}{53/52_{MT}(50/52_{MS} - 50/52_{SP}) + 53/52_{MS}(50/52_{SP} - 50/52_{MT}) + 53/52_{SP}(50/52_{MT} - 50/52_{MS})}$$

$$c = 54/52_{MT} - a53/52_{MT} - b50/52_{MT}$$

11. Repeat steps 5-6 using ST & SA instead of MS & MT:

$$d = \frac{54/52_{SA} - 54/52_{ST}}{53/52_{SA} - 53/52_{ST}}$$

$$e = 54/52_{SA} - d53/52_{SA}$$

$$f = \frac{54/52_{SA} - 54/52_{ST}}{50/52_{SA} - 50/52_{ST}}$$

$$g = 54/52_{SA} - f50/52_{SA}$$

- values for SA were calculated in step 2 using the initial guess for F_{nat}

12. Assign x_{int}, y_{int}, and z_{int} as the new values for SA.

13. Calculate a new value for F_{nat}:

$$F_{nat} = \frac{-\ln(R_{MT}/R_{SA})}{\ln(m_1/m_2)}$$

- use newest values for MT
- use newest values for SA

14. Repeat steps 2-13 iteratively until the value of F_{nat} converges.

   – in each iteration of step 2 use the newest value of F_{nat} calculated in the previous iteration of step 13

15. Calculate contribution (voltage) from interfering elements using the final value of Fins to adjust the isotope ratios:

$$(50Ti)_{calc} = \frac{(49Ti)_{meas} \times \left(\frac{M_{49Ti}}{M_{50Ti}}\right)^{F_{ins}-1}}{\left(\frac{49Ti}{50Ti}\right)_{IUPAC}}$$

$$(50V)_{calc} = \frac{(51V)_{meas} \times \left(\frac{50V}{51V}\right)_{IUPAC}}{\left(\frac{M_{50V}}{M_{51V}}\right)^{F_{ins}-1}}$$

$$(54Fe)_{calc} = \frac{(56Fe)_{meas} \times \left(\frac{54Fe}{56Fe}\right)_{IUPAC}}{\left(\frac{M_{54Fe}}{M_{56Fe}}\right)^{F_{ins}-1}}$$

16. Calculate interference element corrected values (voltages) for ^{50}Cr & ^{54}Cr:

$$(50Cr)_{corrected} = (50Cr)_{meas} - (50Ti)_{calc} - (50V)_{calc}$$

$$(54Cr)_{corrected} = (54Cr)_{meas} - (54Fe)_{calc}$$

17. Calculate interference element corrected Cr isotope ratios (^{53}Cr/^{52}Cr, ^{50}/^{52}Cr, ^{54}/^{52}Cr).

18. Repeat the double spike inversion on the corrected isotope ratios (steps 2-14).

   – final values of SA represent the true Cr isotope ratios of the sample